Chinese Journal of Aeronautics, (2018), xxx(xx): xxx–xxx

Chinese Society of Aeronautics and Astronautics
& Beihang University

Chinese Journal of Aeronautics

cja@buaa.edu.cn
www.sciencedirect.com

Geometric error analysis of an over-constrained parallel tracking mechanism using the screw theory

Jiateng ZHANG [a], **Binbin LIAN** [a,b,*], **Yimin SONG** [a]

[a] *Key Laboratory of Mechanism Theory and Equipment Design of Ministry of Education, Tianjin University, Tianjin 300072, China*
[b] *Department of Machine Design, KTH Royal Institute of Technology, Stockholm SE-10044, Sweden*

Received 3 March 2018; revised 8 April 2018; accepted 13 June 2018

KEYWORDS

Error model simulation;
Geometric error modeling;
Over-constrained parallel mechanism;
Screw theory;
Sensitivity analysis

Abstract This paper deals with geometric error modeling and sensitivity analysis of an over-constrained parallel tracking mechanism. The main contribution is the consideration of over-constrained features that are usually ignored in previous research. The reciprocal property between a motion and a force is applied to tackle this problem in the framework of the screw theory. First of all, a nominal kinematic model of the parallel tracking mechanism is formulated. On this basis, the actual twist of the moving platform is computed through the superposition of the joint twist and geometric errors. The actuation and constrained wrenches of each limb are applied to exclude the joint displacement. After eliminating repeated errors brought by the multiplication of wrenches, a geometric error model of the parallel tracking mechanism is built. Furthermore, two sensitivity indices are defined to select essential geometric errors for future kinematic calibration. Finally, the geometric error model with minimum geometric errors is verified by simulation with SolidWorks software. Two typical poses of the parallel tracking mechanism are selected, and the differences between simulation and calculation results are very small. The results confirm the correctness and accuracy of the geometric error modeling method for over-constrained parallel mechanisms.

1. Introduction

Real-time target tracking systems with high precision are vastly required in industrial, medical, and military domains. Their design and control have become a research hotspot.[1,2] Among the main issues to be tackled, a key problem is the development of a tracking mechanism with a large workspace and a high accuracy.[3,4] Over the past decades, intensive efforts have been made to topological synthesis[5,6] and kinematic analysis and design[7,8] of tracking mechanisms. In this regard, we proposed a 2 rotational Degree-of-Freedom (DoF) Parallel Tracking Mechanism (PTM), as is shown in Fig. 1.[9] It is with

* Corresponding author at: Key Laboratory of Mechanism Theory and Equipment Design of Ministry of Education, Tianjin University, Tianjin 300072, China.
E-mail address: lianbinbin@tju.edu.cn (B. LIAN).

Peer review under responsibility of Editorial Committee of CJA.

ELSEVIER Production and hosting by Elsevier

https://doi.org/10.1016/j.cja.2018.08.021

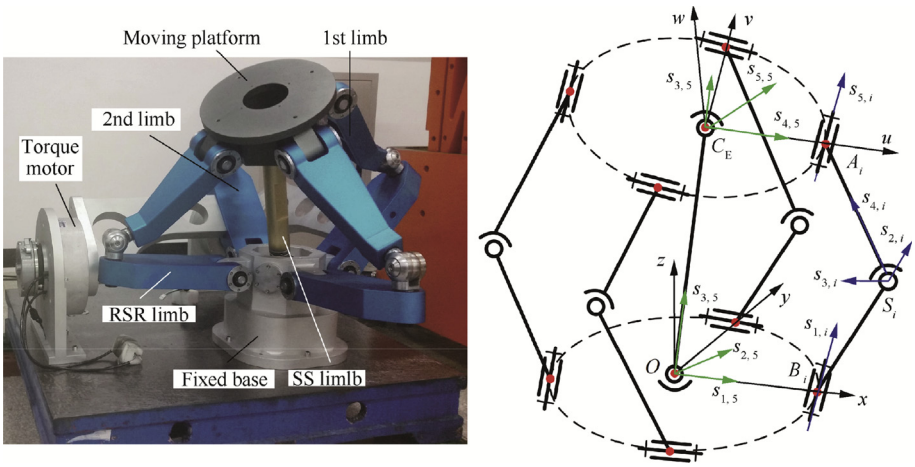

Fig. 1 2-DoF PTM and its schematic diagram.

a symmetrical structure, up to 90° rotational angles, and potentially high stiffness. We assume it as a promising solution for a target tracking system with high precision.[10] Before applying the PTM to build a tracking system, it is found that position and orientation inaccuracies of the PTM have great effects on the precision of tracking trajectory. Therefore, kinematic calibration, the technique to identify and compensate geometric errors, is inevitable to improve the accuracy of the PTM.[11,12] In order to implement kinematic calibration, a thorough understanding of the generation and transmission of component errors is the first step. Furthermore, a comprehensive analysis of the effects from these errors on mechanism accuracy is also necessary.

In the former direction, error modeling between geometric errors of parts and pose errors of the PTM is to be investigated. From the mathematical perspective, geometric errors resulted from a construction process can be described by the deviations of nominal and real kinematic models.[13] To study the actual kinematic features of mechanisms, scholars have applied different mathematical tools in geometric error modeling. Commonly adopted approaches are Denavit-Hartenberg (D-H) convention, the Product-of-Exponential (PoE) formula, and the screw theory.

D-H convention is a matrix-based method. The relative position and orientation of adjacent bodies are described by 4×4 homogeneous transformation matrices. Meanwhile, the nominal kinematic model of a serial limb or mechanism is the successive multiplication of these matrices. The actual kinematic model is formulated by taking small perturbation of every element in each matrix.[14,15] Harb and Burdekin[16] established a geometric error model of a spatial serial manipulator through matrix operations. For the 6-DoF Stewart mechanism, Wang and Masory[17] applied D-H convention to deal with the error model of each serial limb. Similarly, a geometric error analysis of some lower-mobility parallel mechanisms[18,19] was carried out by D-H convention. In most cases, D-H convention is chosen because (1) geometric errors of parts can be included by exhaustive differentiation, and (2) transmissions of geometric errors can be computed by multiplication and summation of matrices. However, it has been pointed out that D-H convention is not applicable for geometric error modeling of a mechanism having collinear adjacent joint axes.[20]

An alternative to tackle the problem is modified models based on D-H matrices, for instance, the six-parameter representation S-model[21] or the continuous and parametrically complete (CPC) model.[22] In these models, two additional parameters are added to allow arbitrary displacements of joint axes. Hence, the singularity problem caused by collinear adjacent joint axes is fixed. Another option is the PoE formula. It can handle kinematic singularity by smoothly changing kinematic parameters. Moreover, different types of joints are uniformly described and modeled.[23] Park and Okamura[24,25] applied global frame representation and formulated an error model of an open-loop manipulator by using the global PoE model. Aiming at a complete, minimal, and continuous error model, Chen et al.[20] combined both global and local PoE formulas to analyze the errors of a serial mechanism. Although both methods are effective for the singular problem caused by collinear axes, the modeling process can be tedious when closed-loop mechanisms like the PTM are involved. This is because displacements from passive joints are included in these methods, making the geometric error model difficult to be directly applied for kinematic calibration.

Being able to describe joint axes in a concise manner, the screw theory has been widely applied in mechanism analysis, including kinematic, stiffness, and dynamics. For the kinematics of parallel mechanisms, motions of joint axes are described by twist, and limb forces are denoted by wrench. Nominal kinematics of parallel mechanisms are computed by the accumulation of joint twist, and the actual kinematic is calculated by linear superposition of joint twist and geometric errors.[26] Joint displacements can be eliminated from geometric error models through the reciprocal property between twist and wrench.[27,28] Along this track, Charker et al.[29] formulated geometric error models of spatial parallel mechanisms and analyzed their position and orientation errors. Kumaraswamy et al.[30] proposed a screw theory-based framework for tolerance analysis of planar and spatial manipulators. By identifying joint displacements as non-compensable errors, Liu et al.[31] investigated a geometric error modeling method of lower-mobility parallel mechanisms through the Jacobian matrix. Also relying on the generalized Jacobian matrix, Sun et al.[32,33] worked on the geometric error analysis of a 3-DoF parallel mechanism, which is of great help in kinematic calibrations.

Please cite this article in press as: ZHANG J et al. Geometric error analysis of an over-constrained parallel tracking mechanism using the screw theory, *Chin J Aeronaut* (2018), https://doi.org/10.1016/j.cja.2018.08.021

The effectiveness of the screw theory in geometric error modeling of parallel mechanisms has been highly recognized. However, little attention has been paid to over-constrained parallel mechanisms.

Over-constrained parallel mechanisms are those that have redundant constraints.[34–37] They are welcomed in practice because their stiffness and operational stability are usually better than those of non-overconstrained mechanisms. For instance, additional constrained forces are applied by two passive limbs in the PTM, and these over-constrained forces contribute to avoidance of kinematic singularity and enhancement of rigidity.[10] An introduction of over constraints is beneficial to the performance of parallel mechanisms, but it also brings difficulties in geometric error modeling by the screw theory. Commonly, a 6×6 non-singular Jacobian matrix consisting actuated and constrained wrenches is applied to eliminate joint displacements in each limb. However, the constrained wrenches of over-constrained parallel mechanisms in the Jacobian matrix are usually equivalent wrenches. They are different from the actual constraints within limbs. An analysis and application of actual wrenches is necessary for accurate geometric error modeling.

What's more, due to the numerous and complicated geometric errors of parts, it remains a difficult task for kinematic calibration. Hence, finding out the main geometric errors is essential for increasing efficiency of kinematic calibration.[38] To this end, sensitivity analysis plays an important role in assessing the effects of geometric errors on mechanism accuracy. Two approaches in terms of analytical and probabilistic methods are involved so far. Through linearization of kinematic equations, Caro et al.[39] worked on the sensitivity analysis of a 3-DoF parallel mechanism. Utilizing an interval analysis method, Wu and Rao[40] obtained sensitivity coefficients of geometric errors from non-linear equations of a parallel mechanism. It has been pointed out that the analytical approach is computationally expensive and only suitable for parallel mechanisms with a simple structure.[41] On the contrary, the probabilistic approach can deal with a large amount of geometric errors in an efficient manner. Sun et al.[32] and Chen et al.[42] assumed geometric errors following a normal distribution, and carried out sensitivity analysis of a 3-DoF parallel mechanism and an SCARA mechanism based on probabilistic models. However, Li et al.[38] mentioned that the probabilistic assumption is hard to guarantee in practical use. In order to efficiently find out the main geometric errors for the PTM, an effective sensitivity analysis method is badly required.

In summary, kinematic calibration is of significance to the development of a target tracking system with high precision. Though substantial progress has been made in geometric error modeling and sensitivity analysis, methods for over-constrained parallel mechanisms are limited or even not appropriate. Taking the PTM as an example, the present study investigates generation and transmission of geometric errors, as well as the sensitivity of these geometric errors to over-constrained parallel mechanisms. Reminder of this paper is as follows. Section 2 briefly introduces the structure of the PTM and formulates its nominal kinematic model by the screw theory. Section 3 carries out geometric error modeling of the PTM and summarizes the general error modeling procedure for over-constrained parallel mechanisms. Sensitivity analysis is implemented to select the essential geometric errors for kinematic calibration in Section 4, while verification of the geometric error model through simulation in SolidWorks software is implemented in Section 5. Conclusions are drawn in Section 6.

2. An over-constrained parallel tracking mechanism and its nominal kinematics

As shown in Fig. 1, the main body of the PTM consists of a fixed base, five limbs (four RSR limbs and one SS limb), and a moving platform. The RSR limbs are formed by a revolute (R) joint, a spherical (S) joint, and then a revolute joint. The SS limb is composed of two spherical joints. The first R joint in the 1st and 2nd limbs is connected to torque motors. The lengths of two links within each limb are required to be the same, and the links among limbs should be identical. The PTM has two rotational capabilities. In a physical prototype, the S joint is replaced by three R joints whose rotational axes are linearly independent. Through such an arrangement, the mobility remains to be the same while rotational angles are bigger.

Some notations and coordinate frames are assigned for the nominal kinematics of the PTM. Centers of the fixed base and the moving platform are denoted by O and C_E, respectively. They are also centers of S joints in the SS limb. Centers of joints within an RSR limb are represented by B_i, S_i, and A_i ($i = 1, 2, 3, 4$) in sequence. Taking point O as the origin, a fixed coordinate frame O-xyz is defined. The x-axis points from point O to point B_1, while the z-axis is perpendicular to the fixed base. A moving coordinate frame C_E-uvw is established at point C_E. Its u-axis is the direction from point C_E to point A_1, and w-axis is normal to the plane of the moving platform. The frames satisfy the right-hand rule. Concerning the geometric constraints, the inverse position formulation of the PTM is derived by Qi et al.[43]. On this basis, its input-output velocity model is firstly carried out by the screw theory in the present study.

Generally, a six-dimensional basis is associated to describe the space of an instantaneous motion (or twist). The elements of the basis are three rotations about and three translations along axes of the Cartesian frame. The basis can also be interpreted as a wrench, in which the basis vectors are pure forces along and moments about the coordinate axes. In fact, wrenches constitute the dual vector space of a twist, i.e., the standard basis of a twist and a wrench forms the basis of a six-dimensional space. The action of a wrench on a twist is the instantaneous work contributed by the wrench during the motion along the twist. This is defined as the reciprocal screw product. If a wrench does not do work on a twist, their reciprocal product is zero, and then the wrench and the twist are described as being reciprocal. The reciprocal product can also be expressed by the generalized inner product if the twist screw is described in axis-coordinate as $\$_t = [\boldsymbol{v}^T, \boldsymbol{\omega}^T]^T = [v_x, v_y, v_z, \omega_x, \omega_y, \omega_z]^T$. Meanwhile, the coordinates of the wrench in the standard basis are denoted by $\$_w = [\boldsymbol{f}^T, \boldsymbol{m}^T]^T = [f_x, f_y, f_z, m_x, m_y, m_z]^T$.

When dealing with an instantaneous motion of parts whose connecting joint is a revolute joint, a twist can be determined by the rotational axis as $\$_t = [\boldsymbol{r}_r \times \boldsymbol{s}_r, \boldsymbol{s}_r]^T$, herein $\boldsymbol{s}_r$ is the vector of the rotational axis and $\boldsymbol{r}_r$ is the vector pointing from the

origin of the coordinate frame to any point on the axis. Similarly, when the connecting joint of parts is a prismatic joint, a twist would be described by the translational axis as $\$_{\mathrm{t}} = [\boldsymbol{s}_{\mathrm{p}}, \boldsymbol{0}]^{\mathrm{T}}$, in which $\boldsymbol{s}_{\mathrm{p}}$ is the vector of the translational axis. It is noted that joints with more than 1 DoF can always be substituted by several 1-DoF joints, and the twist of a serial linkage is derived by the superposition of the 1-DoF joint twists. For the PTM, the twist at point C_{E} can be expressed via RSR and SS limbs as follows:

$$\$_{\mathrm{t}} = \sum_{j=1}^{5} \dot{\theta}_{\mathrm{a},j,i} \hat{\$}_{\mathrm{ta},j,i} \quad i = 1,2,3,4,5 \tag{1}$$

where $\hat{\$}_{\mathrm{ta},j,i}$ and $\dot{\theta}_{\mathrm{a},j,i}$ denote the unit twist screw and its intensity of the jth 1-DoF joint in the ith limb (the SS limb is described as the 5th limb), respectively. Since only R joints are involved in the PTM, it can also be interpreted as the angular velocity $\dot{\theta}_{\mathrm{a},j,i}$ about the joint axis $\hat{\$}_{\mathrm{ta},j,i}$. For an RSR limb, the joint twists are expressed as

$$\begin{cases} \hat{\$}_{\mathrm{ta},1,i} = \begin{bmatrix} \boldsymbol{r}_{\mathrm{CB}_i} \times \boldsymbol{s}_{1,i} \\ \boldsymbol{s}_{1,i} \end{bmatrix} \\ \hat{\$}_{\mathrm{ta},2,i} = \begin{bmatrix} \boldsymbol{r}_{\mathrm{CS}_i} \times \boldsymbol{s}_{2,i} \\ \boldsymbol{s}_{2,i} \end{bmatrix} \\ \hat{\$}_{\mathrm{ta},3,i} = \begin{bmatrix} \boldsymbol{r}_{\mathrm{CS}_i} \times \boldsymbol{s}_{3,i} \\ \boldsymbol{s}_{3,i} \end{bmatrix} \\ \hat{\$}_{\mathrm{ta},4,i} = \begin{bmatrix} \boldsymbol{r}_{\mathrm{CS}_i} \times \boldsymbol{s}_{4,i} \\ \boldsymbol{s}_{4,i} \end{bmatrix} \\ \hat{\$}_{\mathrm{ta},5,i} = \begin{bmatrix} \boldsymbol{r}_{\mathrm{CA}_i} \times \boldsymbol{s}_{5,i} \\ \boldsymbol{s}_{5,i} \end{bmatrix} \end{cases} \quad i = 1,2,3,4$$

where $\boldsymbol{r}_{\mathrm{CB}_i}$, $\boldsymbol{r}_{\mathrm{CS}_i}$, and $\boldsymbol{r}_{\mathrm{CA}_i}$ are the vectors from point C_{E} to points B_i, S_i, and A_i, respectively. $\boldsymbol{s}_{j,i}$ ($j = 1,2,3,4,5$, $i = 1,2,3,4$) denotes the vector of the 1-DoF joint within the RSR limb. The twists are described in the instantaneous frame which is assigned to point C_{E} and parallel to the fixed frame. Similarly, the joint twist in the SS limb is derived as follows:

$$\begin{cases} \hat{\$}_{\mathrm{ta},1,5} = \begin{bmatrix} -\boldsymbol{r} \times \boldsymbol{s}_{1,5} \\ \boldsymbol{s}_{1,5} \end{bmatrix} \\ \hat{\$}_{\mathrm{ta},2,5} = \begin{bmatrix} -\boldsymbol{r} \times \boldsymbol{s}_{2,5} \\ \boldsymbol{s}_{2,5} \end{bmatrix} \\ \hat{\$}_{\mathrm{ta},3,5} = \begin{bmatrix} -\boldsymbol{r} \times \boldsymbol{s}_{3,5} \\ \boldsymbol{s}_{3,5} \end{bmatrix} \\ \hat{\$}_{\mathrm{ta},4,5} = \begin{bmatrix} \boldsymbol{0} \\ \boldsymbol{s}_{4,5} \end{bmatrix} \\ \hat{\$}_{\mathrm{ta},5,5} = \begin{bmatrix} \boldsymbol{0} \\ \boldsymbol{s}_{5,5} \end{bmatrix} \end{cases}$$

where $\boldsymbol{r}$ is the vector from point O to point C_{E}, and $\boldsymbol{s}_{j,5}$ is the vector of the 1-DoF joint within the SS limb.

Referring to the reciprocal properties of a twist and a wrench, the constraint wrench of an RSR limb is obtained by finding out the six-dimensional vector having zero inner products with all the five twists, i.e.,

$$\hat{\$}_{\mathrm{wc},i} = \begin{bmatrix} \boldsymbol{s}_{\mathrm{c},i} \\ \boldsymbol{r}_{\mathrm{CS},i} \times \boldsymbol{s}_{\mathrm{c},i} \end{bmatrix} \quad i = 1,2,3,4 \tag{2}$$

where $\boldsymbol{s}_{\mathrm{c},i} = \boldsymbol{l}_{1,i} \times \boldsymbol{l}_{2,i}$, in which $\boldsymbol{l}_{1,i} = \boldsymbol{s}_{5,i} \times \boldsymbol{r}_{\mathrm{SA},i}$ and $\boldsymbol{l}_{2,i} = \boldsymbol{s}_{1,i} \times \boldsymbol{r}_{\mathrm{BS},i}$.

With the same manner, the constrained wrench of the SS limb is computed as follows:

$$\hat{\$}_{\mathrm{wc},5} = \begin{bmatrix} \boldsymbol{r}/H \\ \boldsymbol{0}_{1\times 3} \end{bmatrix} \tag{3}$$

where H is the length of links SS. By locking the actuated R joint in the 1st RSR limb, the actuated wrench can be obtained from the zero products with the rest four twists and one constrained wrench. Similarly, the actuated wrench of the 2nd RSR limb is derived as

$$\begin{cases} \hat{\$}_{\mathrm{wa},1} = \begin{bmatrix} \boldsymbol{r}_{\mathrm{SA},1}/L \\ \boldsymbol{r}_{\mathrm{CA},1} \times \boldsymbol{r}_{\mathrm{SA},1}/L \end{bmatrix} \\ \hat{\$}_{\mathrm{wa},2} = \begin{bmatrix} \boldsymbol{r}_{\mathrm{SA},2}/L \\ \boldsymbol{r}_{\mathrm{CA},2} \times \boldsymbol{r}_{\mathrm{SA},2}/L \end{bmatrix} \end{cases} \tag{4}$$

where L is the length of links RS, $\boldsymbol{r}_{\mathrm{SA},1}$ are the vectors from point S_1 to point A_1, and $\boldsymbol{r}_{\mathrm{SA},2}$ are the vectors from point S_2 to point A_2.

It is found that two actuated wrenches and five constrained wrenches are applied to the moving platform of the PTM. As the dimension of the Jacobian matrix is 6×6, there is one redundant constrained wrench. Usually redundant wrenches are excluded in the Jacobian matrix, as has been done by Sun et al.[28]. However, not only the wrenches in the full-rank Jacobian matrix but also the exact wrenches in each limb are applied for geometric error modeling in the present study. This is more accurate in the elimination of joint displacements.

3. Geometric error modeling

Geometric errors resulted from the matching and assembling process are described by the deviation of the joint axis. Transmissions of these errors are from the actual joint axis to the limb and then the whole mechanism. Therefore, geometric error modeling starts from an analysis of the actual adjacent joint axes. On this basis, the actual twist of each limb is derived, and the elimination of the passive joint displacement is implemented. Finally, a geometric model of the mechanism is formulated.

Following this procedure, body-fixed reference frames are firstly assigned to the actual joint axes of the PTM for the convenience of analyzing their relation. These frames are denoted by $R_{j,i}$ (i = 1,2,3,4, j = 1,2,...,6). The $z_{j,i}$-axis is the axis of each 1-DoF joint, and the $x_{j,i}$-axis is perpendicular to both the $z_{j,i}$-axis and the $z_{j+1,i}$-axis. The $y_{j,i}$-axis follows the right-hand rule. As is shown in Fig. 2, point $P_{j,i}$ is applied to represent the origin of the frames. Points $P_{1,i}$ and $P_{2,i}$ are the intersections of the $z_{1,i}$-axis and the $x_{1,i}$-axis, the $z_{2,i}$-axis and the $x_{2,i}$-axis, respectively. The other $P_{j,i}$ represents the intersection of the $x_{j-1,i}$-axis and the $z_{j,i}$-axis. The frame on the fixed base $R_{0,i}$ is defined by rotating frame O-xyz about the z-axis with an angle of $(i-1)\pi/2$. The frame on the moving platform is assigned to point C_{E} whose $x_{6,i}$-axis is from point C_{E} to point A_i and the $z_{6,i}$-axis is colinear with the w-axis.

Similarly, body-fixed reference frames $R_{j,5}$ are established for the actual joint axis of the SS limb. The $z_{j,5}$-axis denotes the axis of the jth 1-DoF joint in the SS limb, and the $x_{j,5}$-axis is perpendicular to both the $z_{j,5}$-axis and the $z_{j+1,5}$-axis. The origin point $P_{j,5}$ of frame $R_{j,5}$ is the intersection of the $z_{j,5}$-axis and the $x_{j\text{-}1,5}$-axis, while point $P_{1,5}$ is the intersection

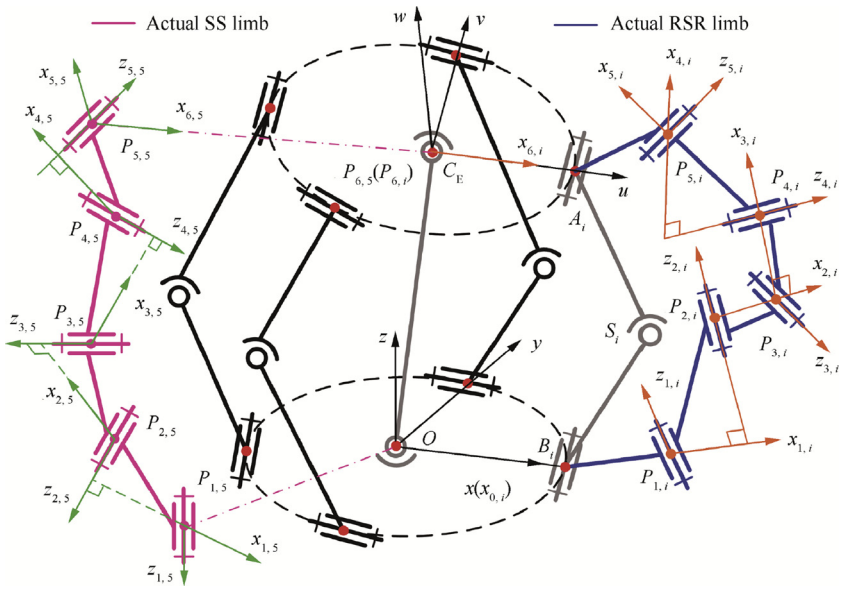

Fig. 2 Actual schematic diagram of RSR and SS limbs.

of the $z_{1,5}$-axis and the $x_{1,5}$-axis. Frame $R_{0,5}$ is just the frame O-xyz, and frame $R_{6,5}$ is coincide with the body-fixed frame C_E-uvw of the moving platform.

With the assigned body-fixed frames, the transformation of actual joint axis can be computed. Then the transformations of geometric errors within limbs are analyzed. It is noted that the four RSR limbs of the PTM are identical. Therefore, geometric error modeling of one RSR limb and the SS limb is demonstrated in the following sections.

3.1. Geometric error model of one RSR limb

Referring to the rotational and translational matrices between coordinate frames, the transformation of the actual joint axis within the ith RSR limb (i = 1,2,3,4) can be described as follows:

$$\begin{cases} {}^{C}\boldsymbol{T}_{O} = \mathrm{Trans}(-\boldsymbol{r}), \\ {}^{O}\boldsymbol{T}_{0,i} = \mathrm{Rot}(z,(i-1)\pi/2),\ i = 1,2,3,4 \\ {}^{0}\boldsymbol{T}_{1,i} = \mathrm{Trans}(x,a)\mathrm{Rot}(x,-\pi/2)\mathrm{Rot}(z,\theta_{1,i}) \\ {}^{1}\boldsymbol{T}_{2,i} = \mathrm{Trans}(x,L\sin\theta_{L})\mathrm{Trans}(y,-L\cos\theta_{L})\cdot \\ \qquad \mathrm{Rot}(x,\pi/2)\mathrm{Rot}(z,\theta_{2,i}+\pi) \\ {}^{2}\boldsymbol{T}_{3,i} = \mathrm{Rot}(x,\pi/2)\mathrm{Rot}(z,\pi/2+\theta_{3,i}), \\ {}^{3}\boldsymbol{T}_{4,i} = \mathrm{Rot}(x,\pi/2)\mathrm{Rot}(z,\theta_{4,i}) \\ {}^{4}\boldsymbol{T}_{5,i} = \mathrm{Trans}(x,L\sin\theta_{H})\mathrm{Trans}(z,L\cos\theta_{H})\cdot \\ \qquad \mathrm{Rot}(x,\pi/2)\mathrm{Rot}(z,\theta_{5,i}+\pi/2) \\ {}^{5}\boldsymbol{T}_{6,i} = \mathrm{Trans}(x,a)\mathrm{Rot}(x,\pi/2)\mathrm{Rot}(z,\pi) \end{cases} \tag{5}$$

where $\mathrm{Trans}(-\boldsymbol{r})$ is the homogeneous transformation matrix of frame O-xyz with respect to instantaneous frame C_E-$x'y'z'$, which is parallel to frame O-xyz. $\mathrm{Trans}(x,y)$ is the homogeneous transformation matrix for the translation along the x-axis with a distance y. $\mathrm{Rot}(x,y)$ is the homogeneous transformation matrix for the rotation about the x-axis with an angle y. a denotes the radius of the moving platform. θ_H and θ_L represent the structural angles of the upper and lower links of an RSR limb, respectively. $\theta_{j,i}$ (j = 1,2,3,4,5, i = 1,2,3,4) denotes a rotational angle about the jth joint axis of the ith RSR limb, which can be solved by inverse kinematic analysis.

Generally, the number for geometric errors of any joint axis should be six, including three position errors along and three orientation errors about the axes of the coordinate frame. However, it has been proven in a previous work that there are redundant errors within a serial limb. These redundant errors are linearly dependent on the other geometric errors.[28] Hence, they would not affect mechanism accuracy independently. As a result, they cannot be identified in kinematic calibration. For this reason, redundant errors are excluded in the geometric error modeling process. For the ith RSR limb (i = 1,2,3,4), all the geometric errors are listed as follows:

$$\begin{cases} {}^{O}\boldsymbol{\Delta}_{1,i} = [{}^{O}\delta x_{1,i},\ {}^{O}\delta y_{1,i},\ {}^{O}\delta z_{1,i},\ {}^{O}\delta\alpha_{1,i},\ 0,\ {}^{O}\delta\gamma_{1,i}]^{T} \\ {}^{1}\boldsymbol{\Delta}_{2,i} = [{}^{1}\delta x_{2,i},\ {}^{1}\delta y_{2,i},\ 0,\ {}^{1}\delta\alpha_{2,i},\ 0,\ 0]^{T} \\ {}^{2}\boldsymbol{\Delta}_{3,i} = [{}^{2}\delta x_{3,i},\ 0,\ 0,\ {}^{2}\delta\alpha_{3,i},\ 0,\ 0]^{T} \\ {}^{3}\boldsymbol{\Delta}_{4,i} = [{}^{3}\delta x_{4,i},\ 0,\ {}^{3}\delta z_{4,i},\ {}^{3}\delta\alpha_{4,i},\ 0,\ 0]^{T} \\ {}^{4}\boldsymbol{\Delta}_{5,i} = [{}^{4}\delta x_{5,i},\ 0,\ {}^{4}\delta z_{5,i},\ {}^{4}\delta\alpha_{5,i},\ 0,\ 0]^{T} \\ {}^{5}\boldsymbol{P}_{6,i}{}^{5}\boldsymbol{\Delta}_{6,i} = -{}^{i}\boldsymbol{A}_{d5,6}\,{}^{6}\boldsymbol{P}_{5,i}\,{}^{6}\boldsymbol{\Delta}_{5,i} \\ {}^{6}\boldsymbol{\Delta}_{5,i} = [{}^{6}\delta x_{5,i},\ {}^{6}\delta y_{5,i},\ {}^{6}\delta z_{5,i},\ {}^{6}\delta\alpha_{5,i},\ 0,\ {}^{6}\delta\gamma_{5,i}]^{T} \end{cases} \tag{6}$$

where ${}^{j-1}\delta x_{j,i}$, ${}^{j-1}\delta y_{j,i}$, and ${}^{j-1}\delta z_{j,i}$ are the position errors of center point $P_{j,i}$ in frame $R_{j,i}$ with respect to frame $R_{j-1,i}$, while ${}^{j-1}\delta\alpha_{j,i}$, ${}^{j-1}\delta\beta_{j,i}$, and ${}^{j-1}\delta\gamma_{j,i}$ are the corresponding orentation errors. In practice, ${}^{5}\boldsymbol{\Delta}_{6,i}$ is replaced by ${}^{6}\boldsymbol{\Delta}_{5,i}$ because it is easier to evaluate the geometric errors of frame $R_{5,i}$ with respect to frame $R_{6,i}$.

With the transformation matrix and defined geometric errors of each joint axis, the actual twist of an RSR limb can be expressed as

$$\$_{t} = \sum_{j=1}^{5}\Delta\theta_{a,j,i}\hat{\$}_{taj,i} + \$_{G,i} \quad i = 1,2,3,4 \tag{7}$$

$$\$_{G,i}=\sum_{j=1}^{5}{}^{i}\mathbf{A}_{dC,j-1}\,{}^{j-1}\mathbf{P}_{j,i}\,{}^{j-1}\Delta_{j,i}+{}^{i}\mathbf{A}_{dC,5}\,{}^{5}\mathbf{P}_{6,i}\,{}^{5}\Delta_{6,i} \tag{8}$$

where $\Delta\theta_{a,j,i}$ denotes the error of $\theta_{a,j,i}$. ${}^{i}\boldsymbol{A}_{dC,j-1}$ is the 6×6 adjoint transformation matrix of frame $R_{j-1,i}$ with respect to frame C_E-$x'y'z'$. ${}^{j-1}\boldsymbol{P}_{j,i}=\begin{bmatrix}\boldsymbol{I}_3 & [{}^{j-1}\boldsymbol{r}_{i,j}\times]\\ \boldsymbol{0}_{3\times3} & \boldsymbol{I}_3\end{bmatrix}$, in which ${}^{j-1}\boldsymbol{r}_{j,i}$ is the position vector of the origin of frame $R_{j,i}$ in frame $R_{j-1,i}$.

Taking the inner product on both sides of Eq. (7) with $\hat{\$}_{wa,i}$ to eliminate the perturbations of passive joints yields

$$\left(\hat{\$}_{wa,i}\right)^{T}\$_t=\hat{\$}_{wa,i}^{T}\hat{\$}_{ta,1,i}\Delta\theta_{a,1,i}+\boldsymbol{E}_{ae,i}\boldsymbol{\varepsilon}_{ae,i}\quad i=1,2 \tag{9}$$

where $\boldsymbol{\varepsilon}_{ae,i}$ is the geometric errors of the ith RSR limb, $\boldsymbol{E}_{ae,i}$ is the relative error coefficient matrices, and

$$\begin{cases}\boldsymbol{E}_{ae,i}=[\lambda x_{a,1,i},\ \lambda y_{a,1,i},\ \lambda z_{a,1,i},\ \lambda\alpha_{a,1,i},\ \lambda\gamma_{a,1,i},\ \lambda x_{a,2,i},\ \lambda y_{a,2,i},\ \lambda x_{a,3,i},\ \cos\theta_{4,i}\sin\theta_H,\\ \qquad \sin\theta_{4,i}\sin\theta_H,\ \sin\theta_H,\ \cos\theta_H,\ \cos(\theta_H+\theta_{5,i}),\ -\sin(\theta_H+\theta_{5,i})]\\ \boldsymbol{\varepsilon}_{ae,i}=[{}^{0}\delta x_{1,i},\ {}^{0}\delta y_{1,i},\ {}^{0}\delta z_{1,i},\ {}^{0}\delta\alpha_{1,i},\ {}^{0}\delta\gamma_{1,i},\ {}^{1}\delta x_{2,i},\ {}^{1}\delta y_{2,i},\ {}^{2}\delta x_{3,i},\ {}^{3}\delta x_{4,i},\ {}^{3}\delta z_{4,i},\\ \qquad {}^{4}\delta x_{5,i},\ {}^{4}\delta z_{5,i},\ {}^{6}\delta x_{5,i},\ {}^{6}\delta z_{5,i}]^{T}\end{cases}$$

herein, the expressions of each element in $\boldsymbol{E}_{ae,i}$ are listed in Appendix A.

Similarly, taking the inner product on both sides of Eq. (7) with $\hat{\$}_{wc,i}$ leads to

$$(\hat{\$}_{wc,i})^{T}\$_t=\boldsymbol{E}_{ce,i}\boldsymbol{\varepsilon}_{ce,i},\quad i=1,2,3,4 \tag{10}$$

where the geometric errors $\boldsymbol{\varepsilon}_{ce,i}$ of the ith RSR limb and the error coefficient matrices $\boldsymbol{E}_{ce,i}$ are expressed as follows:

$$\begin{cases}\boldsymbol{E}_{ce,i}=[\lambda x_{c,1,i},\lambda y_{c,1,i},\lambda z_{c,1,i},\lambda\alpha_{c,1,i},\lambda\gamma_{c,1,i},\lambda x_{c,2,i},\lambda y_{c,2,i},\lambda x_{c,3,i},\lambda x_{c,4,i},\lambda z_{c,4,i},\lambda x_{c,5,i},\\ \qquad \lambda z_{c,5,i},\lambda\alpha_{c,5,i},\lambda x_{c,6,i},\lambda y_{c,6,i},\lambda z_{c,6,i},\lambda\alpha_{c,6,i},\lambda\gamma_{c,6,i}]\\ \boldsymbol{\varepsilon}_{ce,i}=[{}^{0}\delta x_{1,i},{}^{0}\delta y_{1,i},{}^{0}\delta z_{1,i},{}^{0}\delta\alpha_{1,i},{}^{0}\delta\gamma_{1,i},{}^{1}\delta x_{2,i},{}^{1}\delta y_{2,i},{}^{2}\delta x_{3,i},{}^{3}\delta x_{4,i},{}^{3}\delta z_{4,i},{}^{4}\delta x_{5,i},\\ \qquad {}^{4}\delta z_{5,i},{}^{4}\delta\alpha_{5,i},{}^{6}\delta x_{5,i},{}^{6}\delta y_{5,i},{}^{6}\delta z_{5,i},{}^{6}\delta\alpha_{5,i},{}^{6}\delta\gamma_{5,i}]^{T}\end{cases}$$

herein, the expressions of each element in $\boldsymbol{E}_{ce,i}$ are listed in Appendix A.

3.2. Geometric error model of the SS limb

Geometric error modeling of the SS limb is tackled in a similar manner to that of RSR limbs. First of all, the transformation matrices of joint axes are computed as follows:

$$\begin{cases}{}^{C}\boldsymbol{T}_O=\mathrm{Trans}(-\boldsymbol{r}),\ {}^{O}\boldsymbol{T}_{0,5}=\boldsymbol{I}_4\\ {}^{O}\boldsymbol{T}_{1,5}=\mathrm{Rot}(y,\pi/2)\mathrm{Rot}(z,\theta_{1,5}),\\ {}^{1}\boldsymbol{T}_{2,5}=\mathrm{Rot}(x,\pi/2)\mathrm{Rot}(z,\theta_{2,5}-\pi/2)\\ {}^{2}\boldsymbol{T}_{3,5}=\mathrm{Rot}(x,\pi/2)\mathrm{Rot}(z,\pi+\theta_{3,5})\\ {}^{3}\boldsymbol{T}_{4,5}=\mathrm{Trans}(z,H)\mathrm{Rot}(x,\pi/2)\mathrm{Rot}(z,\pi/2+\theta_{4,5})\\ {}^{4}\boldsymbol{T}_{5,5}=\mathrm{Rot}(x,\pi/2)\mathrm{Rot}(z,\theta_{5,5}+\pi/2),\\ {}^{5}\boldsymbol{T}_{6,5}=\mathrm{Rot}(x,\pi/2)\mathrm{Rot}(z,\pi/2)\end{cases} \tag{11}$$

where $\theta_{j,5}$ ($j=1,2,3,4,5$) represents a rotational angle about the jth joint axis of the SS limb. It can also be solved through inverse kinematic analysis.[17]

Geometric errors of each joint in the SS limb are expressed as

$$\begin{cases}{}^{O}\boldsymbol{\Delta}_{1,5}=[{}^{O}\delta x_{1,5},\ {}^{O}\delta y_{1,5},\ {}^{O}\delta z_{1,5},\ 0,\ {}^{O}\delta\beta_{1,5},\ {}^{O}\delta\gamma_{1,5}]^{T}\\ {}^{1}\boldsymbol{\Delta}_{2,5}=[{}^{1}\delta x_{2,5},\ 0,\ 0,\ {}^{1}\delta\alpha_{2,5},\ 0,\ 0]^{T}\\ {}^{2}\boldsymbol{\Delta}_{3,5}=[{}^{2}\delta x_{3,5},\ 0,\ {}^{2}\delta z_{3,5},\ {}^{2}\delta\alpha_{3,5},\ 0,\ 0]^{T}\\ {}^{3}\boldsymbol{\Delta}_{4,5}=[{}^{3}\delta x_{4,5},\ 0,\ {}^{3}\delta z_{4,5},\ {}^{3}\delta\alpha_{4,5},\ 0,\ 0]^{T}\\ {}^{4}\boldsymbol{\Delta}_{5,5}=[{}^{4}\delta x_{5,5},\ 0,\ {}^{4}\delta z_{5,5},\ {}^{4}\delta\alpha_{5,5},\ 0,\ 0]^{T}\\ {}^{5}\boldsymbol{P}_{6,5}\,{}^{5}\boldsymbol{\Delta}_{6,5}=-{}^{5}\boldsymbol{A}_{d5,6}\,{}^{6}\boldsymbol{P}_{5,5}\,{}^{6}\boldsymbol{\Delta}_{5,5}\\ {}^{6}\boldsymbol{\Delta}_{5,5}=[{}^{6}\delta x_{5,5},\ {}^{6}\delta y_{5,5},\ {}^{6}\delta z_{5,5},\ 0,\ {}^{6}\delta\beta_{5,5},\ {}^{6}\delta\gamma_{5,5}]^{T}\end{cases} \tag{12}$$

where ${}^{j-1}\delta x_{j,5}$, ${}^{j-1}\delta y_{j,5}$, and ${}^{j-1}\delta z_{j,5}$ are the position errors of center point $P_{j+1,5}$ in frame $R_{j,5}$ with respect to frame $R_{j-1,5}$. ${}^{j-1}\delta\alpha_{j,5}$, ${}^{j-1}\delta\beta_{j,5}$, and ${}^{j-1}\delta\gamma_{j,5}$ are the corresponding rotational errors.

The actual twist of the SS limb can be obtained by Eqs. (11) and (12) as

$$\$_t=\sum_{j=1}^{5}\Delta\theta_{a,j,5}\hat{\$}_{ta,j,5}+\$_{G,5} \tag{13}$$

$$\$_{G,5}=\sum_{j=1}^{5}{}^{5}\boldsymbol{A}_{dC,j-1}\,{}^{j-1}\boldsymbol{P}_{j,5}\,{}^{j-1}\boldsymbol{\Delta}_{j,5}+{}^{5}\boldsymbol{A}_{dC,5}\,{}^{5}\boldsymbol{P}_{6,5}\,{}^{5}\boldsymbol{\Delta}_{6,5} \tag{14}$$

where $\Delta\theta_{a,j,5}$ denotes the error of $\theta_{a,j,5}$. ${}^{5}\boldsymbol{A}_{dC,j-1}$ is the 6×6 adjoint transformation matrix of frame $R_{j-1,5}$ with respect to frame C_E-$x'y'z'$. ${}^{j-1}\boldsymbol{P}_{j,5}=\begin{bmatrix}\boldsymbol{I}_3 & [{}^{j-1}\boldsymbol{r}_{j,5}\times]\\ \boldsymbol{0}_{3\times3} & \boldsymbol{I}_3\end{bmatrix}$, in which ${}^{j-1}\boldsymbol{r}_{j,5}$ is the position vector of the origin $P_{j,5}$ of frame $R_{j,5}$ in frame $R_{j-1,5}$.

Taking the inner product on both sides of Eq. (8) with $\hat{\$}_{wc,5}$ to eliminate the displacement of passive joints yields

$$\left(\hat{\$}_{wc,5}\right)^{T}\$_t=\boldsymbol{E}_{ce,5}\boldsymbol{\varepsilon}_{ce,5} \tag{15}$$

where the geometric errors $\boldsymbol{\varepsilon}_{ce,5}$ and the error coefficient matrices $\boldsymbol{E}_{ce,5}$ of the SS limb are expressed as follows:

$$\begin{cases} \boldsymbol{E}_{\mathrm{ce},5} = [-\sin\theta_{2,5},\ -\cos\theta_{2,5}\sin\theta_{1,5},\ \cos\theta_{1,5}\cos\theta_{2,5},\ -\cos\theta_{2,5},\ 1,\ \cos\theta_{4,5}, \\ \qquad -\sin\theta_{4,5},\ -\cos\theta_{4,5}\sin\theta_{5,5},\ -\cos\theta_{4,5}\cos\theta_{5,5}] \\ \boldsymbol{\varepsilon}_{\mathrm{ce},5} = [{}^{\mathrm{O}}\delta x_{1,5},\ {}^{\mathrm{O}}\delta y_{1,5},\ {}^{\mathrm{O}}\delta z_{1,5},\ {}^{1}\delta x_{2,5},\ {}^{3}\delta z_{4,5},\ {}^{4}\delta x_{5,5},\ {}^{6}\delta x_{5,5},\ {}^{6}\delta y_{5,5},\ {}^{6}\delta z_{5,5}]^{\mathrm{T}} \end{cases} \tag{16}$$

3.3. Geometric error model of the PTM

During the process of applying wrenches to eliminate joint displacements from the geometric error model of limbs, it is found that some geometric errors are repeatedly included. These repeated errors contribute to the singularity of the error model and result in ambiguity in kinematic calibration. By getting rid of repeated geometric errors, the geometric errors of the PTM are written in a vector form as follows:

$$\boldsymbol{\varepsilon}_{\mathrm{e}} = [\boldsymbol{\varepsilon}_{\mathrm{e},1}^{\mathrm{T}},\ \boldsymbol{\varepsilon}_{\mathrm{e},2}^{\mathrm{T}},\ \boldsymbol{\varepsilon}_{\mathrm{ce},3}^{\mathrm{T}},\ \boldsymbol{\varepsilon}_{\mathrm{ce},4}^{\mathrm{T}},\ \boldsymbol{\varepsilon}_{\mathrm{ce},5}^{\mathrm{T}}]^{\mathrm{T}} \tag{17}$$

where

$$\begin{aligned} \boldsymbol{\varepsilon}_{\mathrm{e},i} = [&\Delta\theta_{\mathrm{a},1,i},\ {}^{\mathrm{O}}\delta x_{1,i},\ {}^{\mathrm{O}}\delta y_{1,i},\ {}^{\mathrm{O}}\delta z_{1,i},\ {}^{\mathrm{O}}\delta\alpha_{1,i},\ {}^{\mathrm{O}}\delta\gamma_{1,i},\ {}^{1}\delta x_{2,i},\ {}^{1}\delta y_{2,i}, \\ &{}^{2}\delta x_{3,i},\ {}^{3}\delta x_{4,i},\ {}^{3}\delta z_{4,i},\ {}^{4}\delta x_{5,i},\ {}^{4}\delta z_{5,i},\ {}^{4}\delta\alpha_{5,i},\ {}^{6}\delta x_{5,i},\ {}^{6}\delta y_{5,i}, \\ &{}^{6}\delta z_{5,i},\ {}^{6}\delta\alpha_{5,i},\ {}^{6}\delta\gamma_{5,i}]^{\mathrm{T}} \quad i = 1,2 \end{aligned}$$

In addition, the relevant error coefficient matrices are modified as follows:

$$\begin{cases} \boldsymbol{J}_{\mathrm{x}} = \begin{bmatrix} \boldsymbol{J}_{\mathrm{xa}} \\ \boldsymbol{J}_{\mathrm{xc}} \end{bmatrix} \\ \boldsymbol{J}_{\mathrm{xa}} = \left[\hat{\$}_{\mathrm{wa},1},\ \hat{\$}_{\mathrm{wa},2}\right]^{\mathrm{T}},\ \boldsymbol{J}_{\mathrm{xc}} = \left[\hat{\$}_{\mathrm{wc},1},\ \hat{\$}_{\mathrm{wc},2},\ \hat{\$}_{\mathrm{wc},3},\ \hat{\$}_{\mathrm{wc},4},\ \hat{\$}_{\mathrm{wc},5}\right]^{\mathrm{T}} \\ \boldsymbol{E}_{\mathrm{e}} = \begin{bmatrix} \boldsymbol{E}_{\mathrm{ae}} \\ \boldsymbol{E}_{\mathrm{ce}} \end{bmatrix} = \begin{bmatrix} \boldsymbol{E}'_{\mathrm{ae},1} & \boldsymbol{0}_{1\times64} & \\ \boldsymbol{0}_{1\times19} & \boldsymbol{E}'_{\mathrm{ae},2} & \boldsymbol{0}_{1\times45} \\ \boldsymbol{E}'_{\mathrm{ce},1} & \boldsymbol{0}_{1\times64} & \\ \boldsymbol{0}_{1\times19} & \boldsymbol{E}'_{\mathrm{ce},2} & \boldsymbol{0}_{1\times45} \\ \boldsymbol{0}_{1\times38} & \boldsymbol{E}_{\mathrm{ce},3} & \boldsymbol{0}_{1\times27} \\ \boldsymbol{0}_{1\times56} & \boldsymbol{E}_{\mathrm{ce},4} & \boldsymbol{0}_{1\times9} \\ \boldsymbol{0}_{1\times74} & \boldsymbol{E}_{\mathrm{ce},5} & \end{bmatrix} \\ \boldsymbol{\varepsilon}_{\mathrm{e}} = \left[\boldsymbol{\varepsilon}_{\mathrm{e},1}^{\mathrm{T}}, \boldsymbol{\varepsilon}_{\mathrm{e},2}^{\mathrm{T}}, \boldsymbol{\varepsilon}_{\mathrm{ce},3}^{\mathrm{T}}, \boldsymbol{\varepsilon}_{\mathrm{ce},4}^{\mathrm{T}}, \boldsymbol{\varepsilon}_{\mathrm{ce},5}^{\mathrm{T}}\right]^{\mathrm{T}} \end{cases}$$

The actual constrained wrenches of each limb are included in the geometric error model. There are more than six wrenches because of the over-constrained features. If we apply the full rank Jacobian as in the previous research, the over-constraints would not be fully considered. It is of importance to eliminate joint displacements at the limb phase for geometric error modeling of over-constrained parallel mechanisms. Multiplying the generalized inverse matrix $(\boldsymbol{J}_{\mathrm{x}}^{\mathrm{T}}\boldsymbol{J}_{\mathrm{x}})^{-1}\boldsymbol{J}_{\mathrm{x}}^{\mathrm{T}}$ to both sides of Eq. (19) yields

$$\begin{cases} \boldsymbol{E}'_{\mathrm{ae},i} = \left[\hat{\$}_{\mathrm{wa},i}^{\mathrm{T}}\hat{\$}_{\mathrm{ta},1,i},\ \lambda x_{\mathrm{a},1,i},\ \lambda y_{\mathrm{a},1,i},\ \lambda z_{\mathrm{a},1,i},\ \lambda\alpha_{\mathrm{a},1,i},\ \lambda\gamma_{\mathrm{a},1,i},\ \lambda x_{\mathrm{a},2,i},\ \lambda y_{\mathrm{a},2,i},\ \lambda x_{\mathrm{a},3,i},\ \cos\theta_{4,i}\sin\theta_{\mathrm{H}},\right. \\ \qquad \left.\sin\theta_{4,i}\sin\theta_{\mathrm{H}},\ \sin\theta_{\mathrm{H}},\ \cos\theta_{\mathrm{H}},\ 0,\ \cos(\theta_{\mathrm{H}}+\theta_{5,i}),\ 0,\ -\sin(\theta_{\mathrm{H}}+\theta_{5,i}),\ 0,\ 0\right] \\ \boldsymbol{E}'_{\mathrm{ce},i} = [0,\ \lambda x_{c,1,i},\ \lambda y_{c,1,i},\ \lambda z_{c,1,i},\ \lambda\alpha_{c,1,i},\ \lambda\gamma_{c,1,i},\ \lambda x_{c,2,i},\ \lambda y_{c,2,i},\ \lambda x_{c,3,i},\ \lambda x_{c,4,i},\ \lambda z_{c,4,i},\ \lambda x_{c,5,i}, \\ \qquad \lambda z_{c,5,i},\ \lambda\alpha_{c,5,i},\ \lambda x_{c,6,i},\ \lambda y_{c,6,i},\ \lambda z_{c,6,i},\ \lambda\alpha_{c,6,i},\ \lambda\gamma_{c,6,i}]^{\mathrm{T}} \end{cases} \quad i = 1,2 \tag{18}$$

Combine the error twists of the five limbs, and rewrite them into a matrix form. The geometric error model of the PTM can be expressed as

$$\boldsymbol{J}_{\mathrm{x}}\$_{\mathrm{t}} = \boldsymbol{E}_{\mathrm{e}}\boldsymbol{\varepsilon}_{\mathrm{e}} \tag{19}$$

where

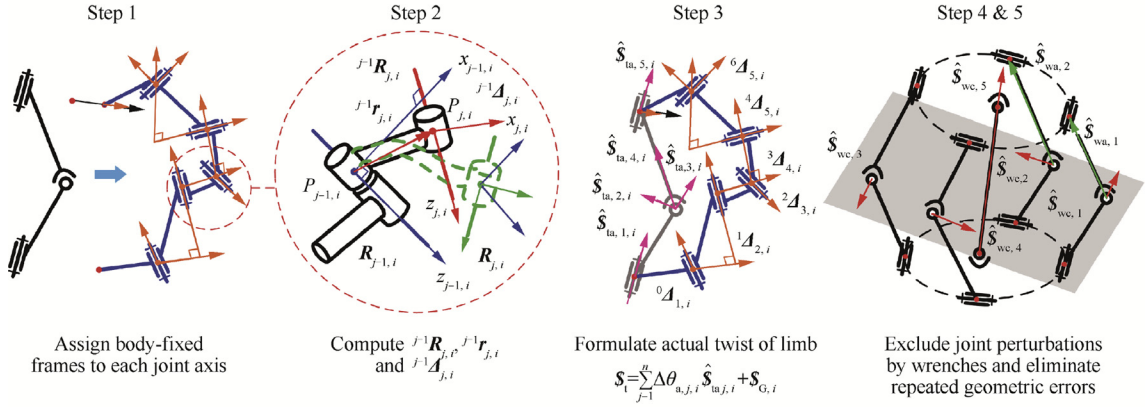

Fig. 3 Geometric error modeling procedure of over-constrained parallel mechanisms.

$$\$_t = (\boldsymbol{J}_x^T \boldsymbol{J}_x)^{-1} \boldsymbol{J}_x^T \boldsymbol{E}_e \boldsymbol{\varepsilon}_e = \boldsymbol{J}_e \boldsymbol{\varepsilon}_e \tag{20}$$

where $\boldsymbol{J}_e$ is the error Jacobian matrix of the PTM. There are 83 geometric errors of parts affecting the pose of the moving platform, including 2 home position errors.

3.4. Geometric error modeling of over-constrained parallel mechanisms

Taking the PTM as an example, the procedure for geometric error modeling of over-constrained parallel mechanisms can be summarized as follows (see Fig. 3).

Step 1: Replace joints within each limb with 1-DoF joints and assign body-fixed frames to joint axes.

Step 2: Compute transformation matrices and define geometric errors between adjacent frames.

Step 3: Formulate the twist of a serial limb by two subsets, joint displacement and geometric errors.

Step 4: Exclude joint displacements by the actual wrenches inserted into the limb.

Step 5: Eliminate repeated geometric errors and combine the twists of all serial limbs to formulate a geometric error model.

The proposed procedure is also applicable to any types of parallel mechanism, including proper constrained and redundant parallel mechanisms.

4. Sensitivity analysis

Before employing the geometric error model in kinematic calibration, sensitivity analysis is carried out to select essential geometric errors. Mechanism errors at the end reference point include position and orientation errors. Since the units are different, it is inappropriate to simultaneously deal with these two subsets of geometric errors in the sensitivity analysis. Based on the geometric error model shown in Eq. (20), the error Jacobian matrix is divided into two sub-matrices corresponding to position and orientation errors, and two local sensitivity indices at a specific configuration are defined as

$$\begin{cases} \mu_{rn} = \sqrt{\sum_{m=1}^{3} J_{e,mn}^2} \\ \mu_{\alpha n} = \sqrt{\sum_{m=4}^{6} J_{e,mn}^2} \end{cases} \tag{21}$$

where $J_{e,mn}$ is the element in the mth row and nth column of $\boldsymbol{J}_e$. $\bar{\mu}_{rn}$ and $\bar{\mu}_{\alpha n}$ denote the position and orientation volumetric errors of the moving platform with respect to the nth geometric error (n = 1,2,3, … ,83), respectively. Herein, volumetric errors are applied to take into account the average errors along or about the x, y, z-axis.

In order to find out the vital geometric errors within the workspace, the global sensitivity indices are given by the average influence of geometric errors in the whole workspace as follows:

$$\begin{cases} \bar{\mu}_{rn} = \int_V \mu_{rn} \mathrm{d}V / V \\ \bar{\mu}_{\alpha n} = \int_V \mu_{\alpha n} \mathrm{d}V / V \end{cases} \tag{22}$$

where V represents the workspace.

Therefore, a sensitivity analysis of the PTM can be conducted by Eq. (22). For the PTM shown in Fig. 1, the circumradius of the moving platform and the fixed base is 150 mm. The length of the link within an RSR limb is 317 mm, while that of the SS limb is 402 mm. Its orientation workspace is denoted by the azimuth angle φ and the tilt angle θ, and $\theta \in [0°, 60°]$, $\varphi \in [0°, 360°]$. Inspired by the statistic method, the workspace is discretized by 10°. In total, 217 poses are derived. Through calculating position and orientation errors at each pose by Eq. (21) and then computing the average, the global sensitivity indices ($\bar{\mu}_r$ and $\bar{\mu}_\alpha$) are obtained, as are shown in Figs. 4 and 5, respectively.

From the sensitivity analysis of the PTM, it is found out that the home position error $\Delta\theta_{a,1,i}$ (i = 1,2), rotational errors

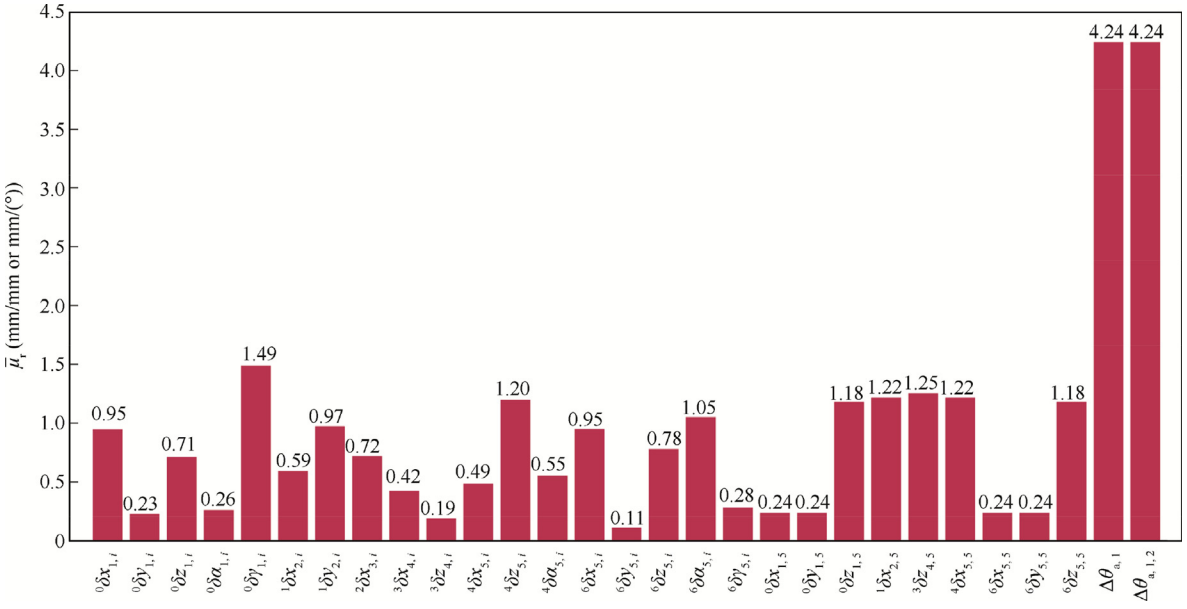

Fig. 4 Sensitivity of geometric errors to position volumetric errors μ_r.

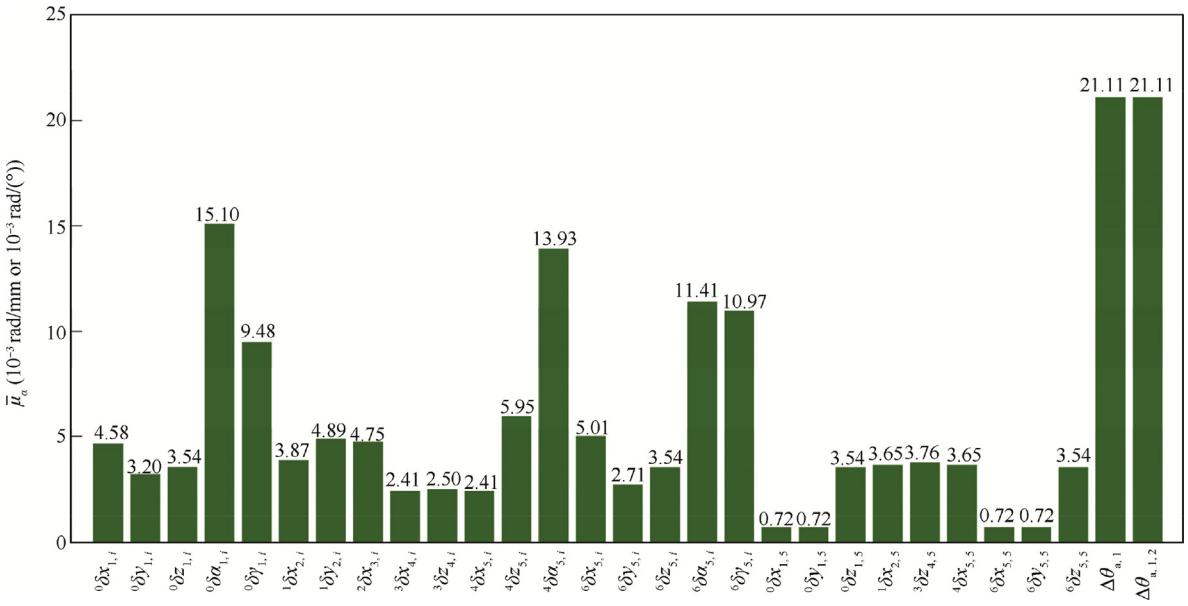

Fig. 5 Sensitivity of geometric errors to orientation volumetric errors μ_α.

such as $^0\delta\alpha_{1,i}$, $^0\delta\gamma_{1,i}$, $^4\delta\alpha_{5,i}$, $^5\delta\alpha_{6,i}$, and $^5\delta\gamma_{6,i}$, and translational errors such as $^0\delta x_{1,i}$, $^0\delta z_{1,i}$, $^1\delta x_{2,i}$, $^1\delta y_{2,i}$, $^4\delta z_{5,i}$, $^5\delta x_{6,i}$, $^5\delta z_{6,i}$, $^0\delta z_{1,5}$, $^1\delta x_{2,5}$, $^3\delta z_{4,5}$, $^4\delta x_{5,5}$, and $^6\delta z_{5,5}$ ($i = 1,2,3,4$) all have great effects on the position volumetric error $\bar{\mu}_r$ and the orientation volumetric error $\bar{\mu}_\alpha$. The number of essential geometric errors is 53. On the other hand, there are some other geometric errors having little influence on the accuracy of the end reference point, such as $^3\delta z_{4,i}$, $^6\delta y_{5,i}$, $^0\delta x_{1,5}$, $^0\delta y_{1,5}$, $^6\delta x_{5,5}$, and $^6\delta y_{5,5}$.

5. Verification of the geometric error model

In this section, the computed geometric error model of the PTM is verified by SolidWorks software. By introducing geometric errors to a virtual prototype of the PTM, the measured coordinates from SolidWorks are compared with those from the geometric error model. By giving certain values to the inputs of the PTM, the virtual prototype built by SolidWorks would drive to the expected pose without errors, which indicates that the virtual prototype is ideal. Through introducing geometric errors to the virtual prototype, the moving platform will deviate from the expected pose, and the measured pose errors will be applied to compare with the calculated pose errors under the same geometric errors. In this way, the geometric error model is verified if the two results are close.

Geometric errors are firstly given in Table 1. Define $\boldsymbol{R}_{\mathrm{M}}$ and $\boldsymbol{R}_{\mathrm{T}}$ as the measured and theoretical orientation matrices of frame C_{E}-uvw with respect to frame O-xyz. Assign $\boldsymbol{a}_{\mathrm{m}}$ and $\boldsymbol{a}_{\mathrm{t}}$ as the measured and theoretical position vectors of point P_1 in frame O-xyz. $\|\delta\boldsymbol{r}_{\mathrm{M}}\|$ and $\|\delta\boldsymbol{\alpha}_{\mathrm{M}}\|$ are the position and orientation volumetric errors obtained by SolidWorks, while

Table 1 Given values of geometric errors.

No.	Error	Value	No.	Error	Value
1	$^0\delta x_{1,1}$	–1.5 mm	15	$^6\delta y_{5,1}$	1.3 mm
2	$^0\delta y_{1,1}$	1.3 mm	16	$^6\delta z_{5,1}$	1.2 mm
3	$^0\delta z_{1,1}$	−1 mm	17	$^6\delta\alpha_{5,1}$	0.1°
4	$^0\delta\alpha_{1,1}$	0.1°	18	$^6\delta\gamma_{5,1}$	−0.1°
5	$^0\delta\gamma_{1,1}$	−0.1°	19	$^0\delta x_{1,5}$	1.1 mm
6	$^1\delta x_{2,1}$	1.6 mm	20	$^0\delta y_{1,5}$	−1.3 mm
7	$^1\delta y_{2,1}$	1.1 mm	21	$^0\delta z_{1,5}$	−1.4 mm
8	$^2\delta x_{3,1}$	1.2 mm	22	$^1\delta x_{2,5}$	−1.4 mm
9	$^3\delta x_{4,1}$	−1.1 mm	23	$^3\delta z_{4,5}$	−1.2 mm
10	$^3\delta z_{4,1}$	0.5 mm	24	$^4\delta x_{5,5}$	1.6 mm
11	$^4\delta x_{5,1}$	−1.3 mm	25	$^6\delta x_{5,5}$	1.2 mm
12	$^4\delta z_{5,1}$	1.7 mm	26	$^6\delta y_{5,5}$	−1.1 mm
13	$^4\delta\alpha_{5,1}$	0.01°	27	$^6\delta z_{5,5}$	−1.3 mm
14	$^6\delta x_{5,1}$	1.4 mm	28	$\Delta\theta_{a1,1}$	1°

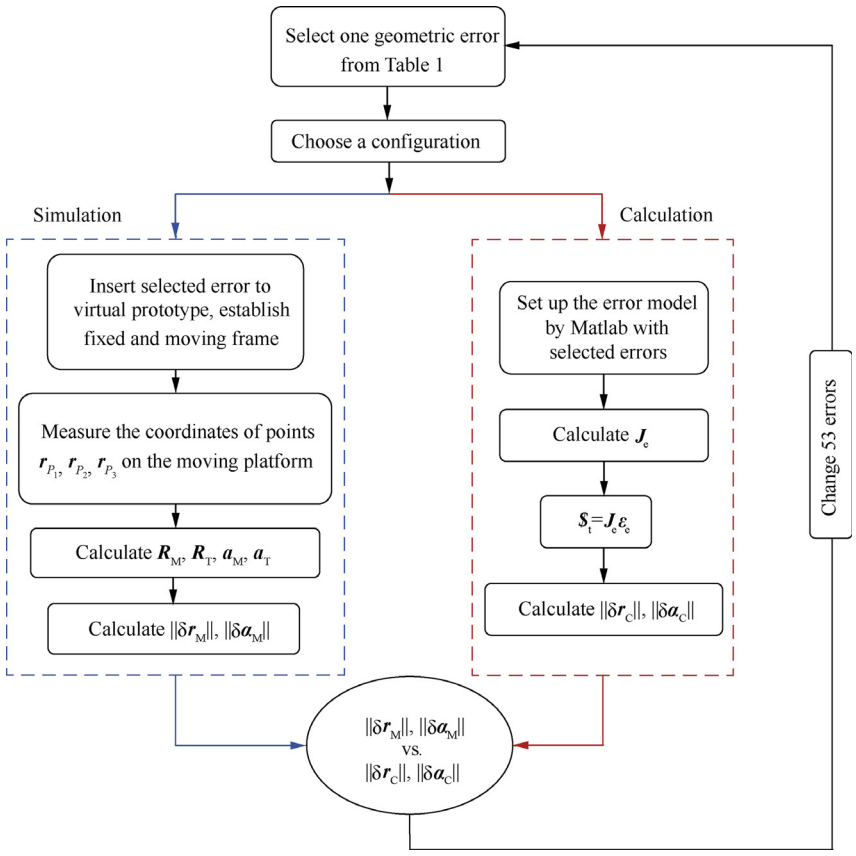

Fig. 6 Verification procedure of the geometric error model.

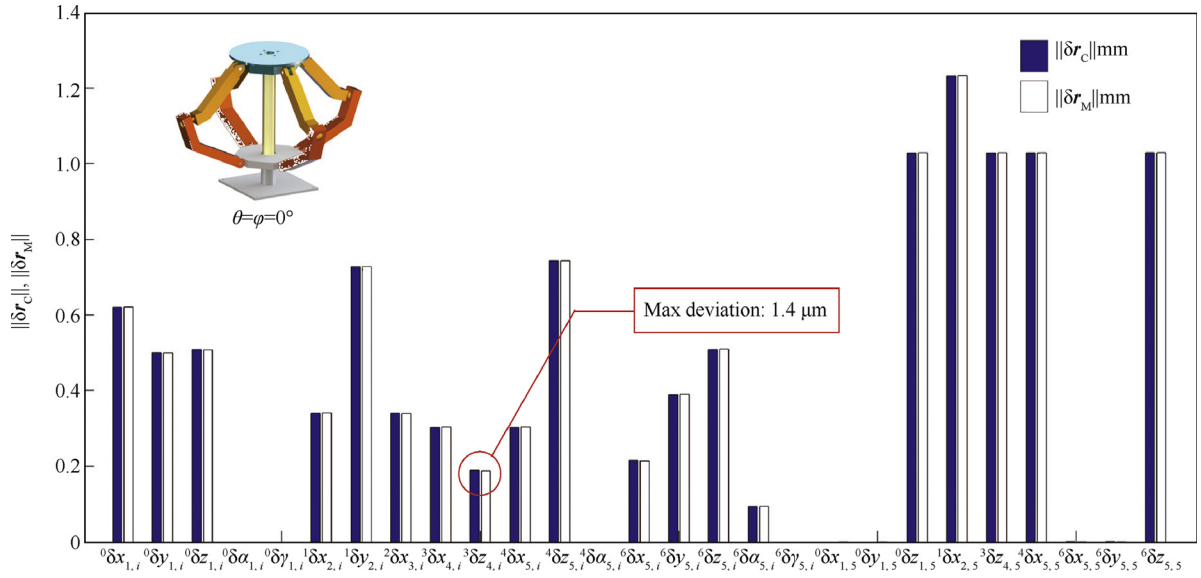

Fig. 7 Verification of position errors ($\varphi = \theta = 0°$).

$\|\delta \boldsymbol{r}_C\|$ and $\|\delta \boldsymbol{\alpha}_C\|$ are the calculated position and orientation errors from the geometric error model. The verification process is implemented as is shown in Fig. 6, which is summarized as follows.

1) Select one geometric error from Table 1 and assign the other errors in $\boldsymbol{\varepsilon}_e$ to be zero. The given error is set to be larger than its possible value for the convenience of verification.

Please cite this article in press as: ZHANG J et al. Geometric error analysis of an over-constrained parallel tracking mechanism using the screw theory, *Chin J Aeronaut* (2018), https://doi.org/10.1016/j.cja.2018.08.021

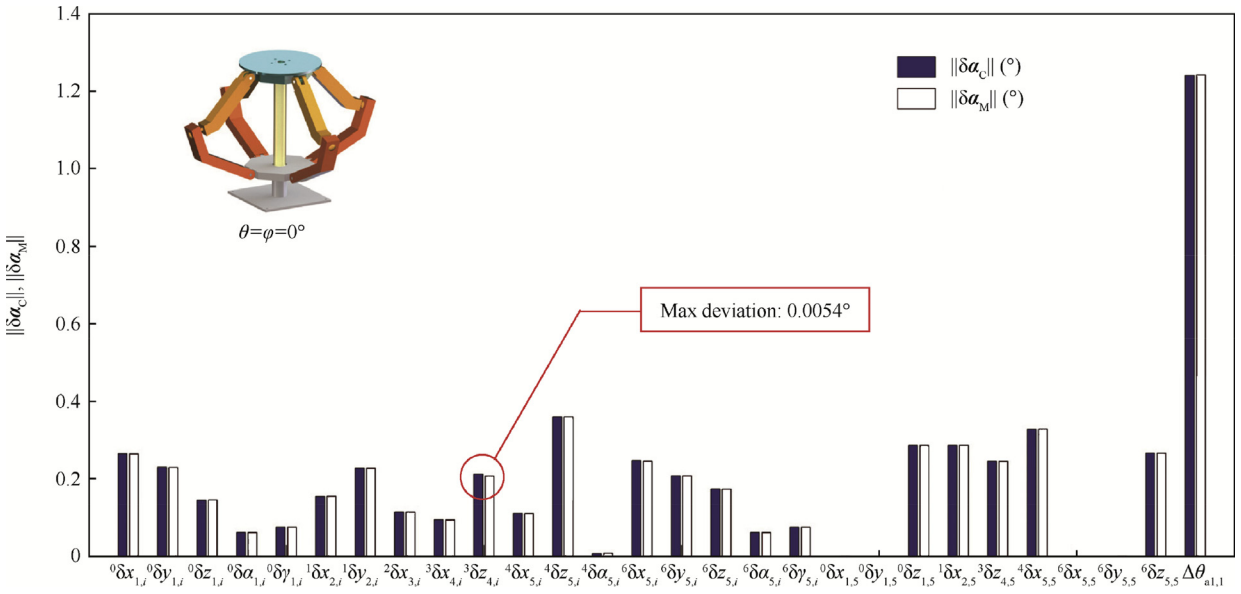

Fig. 8 Verification of orientation errors ($\varphi = \theta = 0°$).

2) Choose a typical pose within the workspace ($\varphi = \theta = 0°$ or $\varphi = 20°, \theta = 15°$).
3) Obtain position and orientation errors of the end reference point in SolidWorks with the selected geometric errors in step 1 under the given configuration in step 2. Firstly, the selected geometric errors are inserted into the virtual prototype. A fixed frame and a moving reference frame are established. Then the moving platform is driven to the given configuration. Moreover, the coordinates of three non-collinear points P_1, P_2, and P_3 are measured. The u-axis is decided by points P_1 and P_2, while the w-axis is determined by points P_1, P_2, and P_3. Hence, $\boldsymbol{R}_M$, $\boldsymbol{R}_T$, $\boldsymbol{a}_m$, and $\boldsymbol{a}_t$ are obtained, with which $\|\delta\boldsymbol{r}_M\|$ and $\|\delta\boldsymbol{\alpha}_M\|$ can be formulated.
4) Derive position and orientation errors of the end reference point calculated by the geometric error model with the selected geometric errors in step 1 under the given configuration in step 2. The geometric error model is programed by Matlab software. $\|\delta\boldsymbol{r}_C\|$ and $\|\delta\boldsymbol{\alpha}_C\|$ can be achieved by setting the selected geometric errors under the given configuration.
5) Compare the simulation results from step 3 with the calculation results from step 4.
6) Go back to step 1. Choose another geometric error and repeat Step 1 to Step 5.

Fig. 7 shows the position volumetric errors of the verification process when $\varphi = \theta = 0°$. The blue bars are calculated position volumetric errors $\|\delta\boldsymbol{r}_C\|$, while the red bars are position volumetric errors $\|\delta\boldsymbol{r}_M\|$ obtained from SolidWorks. The maximum deviation between $\|\delta\boldsymbol{r}_C\|$ and $\|\delta\boldsymbol{r}_M\|$ is 1.4 μm. Fig. 8 illustrates a comparison of orientation volumetric errors when $\varphi = \theta = 0°$. The blue bars are calculated orientation volumetric errors $\|\delta\boldsymbol{\alpha}_C\|$, and the red bars are orientation volumetric errors $\|\delta\boldsymbol{\alpha}_M\|$ from SolidWorks. The maximum deviation between $\|\delta\boldsymbol{\alpha}_C\|$ and $\|\delta\boldsymbol{\alpha}_M\|$ is 0.0054°. Tables 2 and 3 show comparisons of position and orientation errors when $\varphi = 20°, \theta = 15°$. The maximum deviations are 5.8 μm and −0.0063°, respectively. The differences from SolidWorks and calculation are very small. The accuracy of the geometric error model of the PTM is confirmed, and the proposed geometric error modeling method is proven to be effective.

Table 2 Verification of position errors ($\varphi = 20°$, $\theta = 15°$).

No.	Error	$\|\delta\boldsymbol{r}_C\|$ (mm)	$\|\delta\boldsymbol{r}_M\|$ (mm)	$\|\delta\boldsymbol{r}_C\| - \|\delta\boldsymbol{r}_M\|$ (mm)
1	${}^0\delta x_{1,1}$	0.9519	0.9477	0.0042
2	${}^0\delta y_{1,1}$	0.5480	0.5503	−0.0023
3	${}^0\delta z_{1,1}$	0.5754	0.5776	−0.0021
4	${}^0\delta\alpha_{1,1}$	0.1101	0.1102	-1.1×10^{-4}
5	${}^0\delta\gamma_{1,1}$	0.8147	0.8146	1.2×10^{-4}
6	${}^1\delta x_{2,1}$	0.7514	0.7545	−0.0031
7	${}^1\delta y_{2,1}$	0.7879	0.7870	9.2658×10^{-4}
8	${}^2\delta x_{3,1}$	0.9134	0.9128	6.0×10^{-4}
9	${}^3\delta x_{4,1}$	0.6324	0.6315	9.0×10^{-4}
10	${}^3\delta z_{4,1}$	0.2785	0.2793	-8.0×10^{-4}
11	${}^4\delta x_{5,1}$	0.4195	0.4159	0.0036
12	${}^4\delta z_{5,1}$	1.3479	1.3475	4.2840×10^{-4}
13	${}^4\delta\alpha_{5,1}$	0.0216	0.0217	-3.6850×10^{-5}
14	${}^6\delta x_{5,1}$	1.0563	1.0516	0.0048
15	${}^6\delta y_{5,1}$	0.5502	0.5481	0.0021
16	${}^6\delta z_{5,1}$	0.4846	0.4841	5.2050×10^{-4}
17	${}^6\delta\alpha_{5,1}$	0.1952	0.1950	0.0002
18	${}^6\delta\gamma_{5,1}$	0.2064	0.2068	-3.9271×10^{-4}
19	${}^0\delta x_{1,5}$	0.1673	0.1658	0.0015
20	${}^0\delta y_{1,5}$	0.0720	0.0744	−0.0024
21	${}^0\delta z_{1,5}$	1.7211	1.7200	0.0011
22	${}^1\delta x_{2,5}$	1.4319	1.4327	−0.0008
23	${}^3\delta z_{4,5}$	1.4880	1.4867	0.0013
24	${}^4\delta x_{5,5}$	1.1569	1.1580	−0.0011
25	${}^6\delta x_{5,5}$	0.1825	0.1807	0.0018
26	${}^6\delta y_{5,5}$	0.0609	0.0626	−0.0018
27	${}^6\delta z_{5,5}$	1.5982	1.5991	-9.4558×10^{-4}
28	$\Delta\theta_{a1,1}$	4.4637	4.4579	0.0058

Table 3 Verification of orientation errors ($\varphi = 20°$, $\theta = 15°$).

No.	Error	$\|\delta\boldsymbol{\alpha}_C\|$ (°)	$\|\delta\boldsymbol{\alpha}_M\|$ (°)	$\|\delta\boldsymbol{\alpha}_C\| - \|\delta\boldsymbol{\alpha}_M\|$ (°)
1	${}^0\delta x_{1,1}$	0.2718	0.2737	-0.0019
2	${}^0\delta y_{1,1}$	0.2848	0.2847	6.4436×10^{-5}
3	${}^0\delta z_{1,1}$	0.1639	0.1640	-2.6463×10^{-5}
4	${}^0\delta\alpha_{1,1}$	0.0572	0.0573	-7.1164×10^{-5}
5	${}^0\delta\gamma_{1,1}$	0.0906	0.0905	1.270×10^{-5}
6	${}^1\delta x_{2,1}$	0.2181	0.2196	-0.0015
7	${}^1\delta y_{2,1}$	0.2242	0.2241	4.3967×10^{-5}
8	${}^2\delta x_{3,1}$	0.2159	0.2155	4.0×10^{-4}
9	${}^3\delta x_{4,1}$	0.1947	0.1943	4.2×10^{-4}
10	${}^3\delta z_{4,1}$	0.3129	0.3075	0.0054
11	${}^4\delta x_{5,1}$	0.1197	0.1199	-1.1104×10^{-4}
12	${}^4\delta z_{5,1}$	0.3876	0.3882	-5.6234×10^{-4}
13	${}^4\delta\alpha_{5,1}$	0.0112	0.0112	-2.5629×10^{-6}
14	${}^6\delta x_{5,1}$	0.3038	0.3030	7.7082×10^{-4}
15	${}^6\delta y_{5,1}$	0.2835	0.2844	-8.9497×10^{-4}
16	${}^6\delta z_{5,1}$	0.1394	0.1395	-1.0769×10^{-4}
17	${}^6\delta\alpha_{5,1}$	0.1612	0.0613	-3.4×10^{-4}
18	${}^6\delta\gamma_{5,1}$	0.1063	0.1064	-4.4252×10^{-5}
19	${}^0\delta x_{1,5}$	0.0282	0.0286	-3.8392×10^{-4}
20	${}^0\delta y_{1,5}$	0.0121	0.0128	-6.6948×10^{-4}
21	${}^0\delta z_{1,5}$	0.2901	0.2963	-0.0062
22	${}^1\delta x_{2,5}$	0.3571	0.3573	-1.8×10^{-4}
23	${}^3\delta z_{4,5}$	0.2508	0.2562	-0.0054
24	${}^4\delta x_{5,5}$	0.3781	0.3784	-2.7×10^{-4}
25	${}^6\delta x_{5,5}$	0.0308	0.0312	-3.9499×10^{-4}
26	${}^6\delta y_{5,5}$	0.0103	0.0108	-5.1971×10^{-4}
27	${}^6\delta z_{5,5}$	0.2694	0.2757	-0.0063
28	$\Delta\theta_{a1,1}$	1.2724	1.2719	4.3911×10^{-4}

6. Conclusions

This paper deals with geometric error modeling and sensitivity analysis of an over-constrained parallel mechanism based on the screw theory. Conclusions are drawn as follows:

(1) A nominal kinematic model is established by the reciprocal property of the screw theory. Instead of formulating a full rank Jacobian matrix, the actual actuation and constraint wrenches of each limb are computed.

(2) The actual twist of the PTM is computed by each RSR limb and the SS limb. It is the superposition of joint twists and geometric errors within limbs. Body-fixed reference frames are assigned to the actual joint axis. Geometric errors are expressed as deviations of nominal and actual joint axes, and their transmissions are conducted by transformation matrices. Then the actuation and constraint wrenches are applied to exclude joint displacements, and the repeated geometric errors brought by the exclusion are eliminated. Through this geometric error modeling process, the generation and transmission of geometric errors of over-constrained parallel mechanisms are clearly defined and computed.

(3) In the light of an error Jacobian matrix, global sensitivity indices are defined, and a sensitivity analysis of the PTM is carried out. 53 geometric errors are selected from the original 83 errors, which helps increase the efficiency in future kinematic calibration. Finally, the geometric error model with minimum errors is verified by SolidWorks software. Results confirm the correctness of the proposed geometric error modeling method. The proposed geometric error modeling method can also be applied to other types of parallel mechanisms.

Acknowledgments

This research work was supported by the National Natural Science Foundation of China [No. 51475321], Tianjin Research Program of Application Foundation and Advanced Technology [No. 15JCZDJC38900 and 16JCYBJC19300], and the International Postdoctoral Exchange Fellowship Program [No. 32 Document of OCPC, 2017].

Appendix A

The expressions of each element in $\boldsymbol{E}_{ae,i}$ are shown as follows:

$$\begin{cases}
\lambda x_{a,1,i} = \sin\theta_{1,i}(\cos\theta_H \sin\theta_{3,i} + \cos\theta_{3,i}\cos\theta_{4,i}\sin\theta_H) - \cos\theta_{1,i}(\sin\theta_{2,i}\sin\theta_{4,i}\sin\theta_H \\
\qquad + \cos\theta_{2,i}(\cos\theta_{3,i}\cos\theta_H - \cos\theta_{4,i}\sin\theta_{3,i}\sin\theta_H)) \\
\lambda y_{a,1,i} = -\cos\theta_{3,i}\cos\theta_H \sin\theta_{2,i} + \sin\theta_H(\cos\theta_{4,i}\sin\theta_{2,i}\sin\theta_{3,i} + \cos\theta_{2,i}\sin\theta_{4,i}) \\
\lambda z_{a,1,i} = \sin\theta_{1,i}\sin\theta_{2,i}\sin\theta_{4,i}\sin\theta_H + \cos\theta_{1,i}(\cos\theta_H \sin\theta_{3,i} + \cos\theta_{3,i}\cos\theta_{4,i}\sin\theta_H) \\
\qquad + \cos\theta_{2,i}\sin\theta_{1,i}(\cos\theta_{3,i}\cos\theta_H - \cos\theta_{4,i}\sin\theta_{3,i}\sin\theta_H) \\
\lambda\alpha_{a,1,i} = L\cos(\theta_{1,i} + \theta_L)(\cos\theta_{3,i}\cos\theta_H \sin\theta_{2,i} - \sin\theta_H(\cos\theta_{4,i}\sin\theta_{2,i}\sin\theta_{3,i} + \cos\theta_{2,i}\sin\theta_{4,i})) \\
\lambda\gamma_{a,1,i} = -L\sin(\theta_{1,i} + \theta_L)(\cos\theta_{3,i}\cos\theta_H \sin\theta_{2,i} - \sin\theta_H(\cos\theta_{4,i}\sin\theta_{2,i}\sin\theta_{3,i} + \cos\theta_{2,i}\sin\theta_{4,i})) \\
\lambda x_{a,2,i} = -\sin\theta_{2,i}\sin\theta_{4,i}\sin\theta_H + \cos\theta_{2,i}(-\cos\theta_{3,i}\cos\theta_H + \cos\theta_{4,i}\sin\theta_{3,i}\sin\theta_H) \\
\lambda y_{a,2,i} = -\cos\theta_H \sin\theta_{3,i} - \cos\theta_{3,i}\cos\theta_{4,i}\sin\theta_H \\
\lambda x_{a,3,i} = \cos\theta_{3,i}\cos\theta_H - \cos\theta_{4,i}\sin\theta_{3,i}\sin\theta_H
\end{cases} \tag{A1}$$

The expressions of each element in $\boldsymbol{E}_{\mathrm{ce},i}$ are shown as follows:

$$\begin{cases}
\lambda x_{\mathrm{c},1,i} = -\sin(\theta_{1,i}+\theta_{\mathrm{L}})(\cos\theta_{4,i}\cos\theta_{\mathrm{H}}\sin\theta_{2,i}\sin\theta_{3,i}+\cos\theta_{2,i}\cos\theta_{\mathrm{H}}\sin\theta_{4,i}+\cos\theta_{3,i}\sin\theta_{2,i}\sin\theta_{\mathrm{H}}) \\
\lambda y_{\mathrm{c},1,i} = -\cos\theta_{\mathrm{L}}\sin\theta_{3,i}\sin\theta_{\mathrm{H}}+\cos\theta_{\mathrm{H}}\sin\theta_{\mathrm{L}}(\cos\theta_{2,i}\cos\theta_{4,i}\sin\theta_{3,i}-\sin\theta_{2,i}\sin\theta_{4,i}) \\
\qquad +\cos\theta_{3,i}(\cos\theta_{4,i}\cos\theta_{\mathrm{H}}\cos\theta_{\mathrm{L}}+\cos\theta_{2,i}\sin\theta_{\mathrm{H}}\sin\theta_{\mathrm{L}}) \\
\lambda z_{\mathrm{c},1,i} = -\cos(\theta_{1,i}+\theta_{\mathrm{L}})(\cos\theta_{4,i}\cos\theta_{\mathrm{H}}\sin\theta_{2,i}\sin\theta_{3,i}+\cos\theta_{2,i}\cos\theta_{\mathrm{H}}\sin\theta_{4,i}+\cos\theta_{3,i}\sin\theta_{2,i}\sin\theta_{\mathrm{H}}) \\
\lambda \alpha_{\mathrm{c},1,i} = -L\cos(\theta_{1,i}+\theta_{\mathrm{L}})(-\cos\theta_{\mathrm{L}}\sin\theta_{3,i}\sin\theta_{\mathrm{H}}+\cos\theta_{\mathrm{H}}\sin\theta_{\mathrm{L}}(\cos\theta_{2,i}\cos\theta_{4,i}\sin\theta_{3,i}-\sin\theta_{2,i}\sin\theta_{4,i}) \\
\qquad +\cos\theta_{3,i}(\cos\theta_{4,i}\cos\theta_{\mathrm{H}}\cos\theta_{\mathrm{L}}+\cos\theta_{2,i}\sin\theta_{\mathrm{H}}\sin\theta_{\mathrm{L}})) \\
\lambda \gamma_{\mathrm{c},1,i} = L\sin(\theta_{1,i}+\theta_{\mathrm{L}})(-\cos\theta_{\mathrm{L}}\sin\theta_{3,i}\sin\theta_{\mathrm{H}}+\cos\theta_{\mathrm{H}}\sin\theta_{\mathrm{L}}(\cos\theta_{2,i}\cos\theta_{4,i}\sin\theta_{3,i}-\sin\theta_{2,i}\sin\theta_{4,i}) \\
\qquad +\cos\theta_{3,i}(\cos\theta_{4,i}\cos\theta_{\mathrm{H}}\cos\theta_{\mathrm{L}}+\cos\theta_{2,i}\sin\theta_{\mathrm{H}}\sin\theta_{\mathrm{L}})) \\
\lambda x_{\mathrm{c},2,i} = -\sin\theta_{\mathrm{L}}(\cos\theta_{4,i}\cos\theta_{\mathrm{H}}\sin\theta_{2,i}\sin\theta_{3,i}+\cos\theta_{2,i}\cos\theta_{\mathrm{H}}\sin\theta_{4,i}+\cos\theta_{3,i}\sin\theta_{2,i}\sin\theta_{\mathrm{H}}) \\
\lambda y_{\mathrm{c},2,i} = \cos\theta_{\mathrm{L}}(\cos\theta_{4,i}\cos\theta_{\mathrm{H}}\sin\theta_{2,i}\sin\theta_{3,i}+\cos\theta_{2,i}\cos\theta_{\mathrm{H}}\sin\theta_{4,i}+\cos\theta_{3,i}\sin\theta_{2,i}\sin\theta_{\mathrm{H}}) \\
\lambda x_{\mathrm{c},3,i} = -\cos\theta_{3,i}\cos\theta_{4,i}\cos\theta_{\mathrm{H}}\cos\theta_{\mathrm{L}}\sin\theta_{2,i}+\cos\theta_{\mathrm{L}}\sin\theta_{2,i}\sin\theta_{3,i}\sin\theta_{\mathrm{H}}+\cos\theta_{\mathrm{H}}\sin\theta_{4,i}\sin\theta_{\mathrm{L}} \\
\lambda x_{\mathrm{c},4,i} = -\cos\theta_{2,i}\cos\theta_{3,i}\cos\theta_{\mathrm{H}}\cos\theta_{\mathrm{L}}\sin\theta_{4,i}-\cos\theta_{\mathrm{L}}\sin\theta_{2,i}\sin\theta_{\mathrm{H}}-\cos\theta_{\mathrm{H}}\sin\theta_{3,i}\sin\theta_{4,i}\sin\theta_{\mathrm{L}} \\
\lambda z_{\mathrm{c},4,i} = \cos\theta_{2,i}\cos\theta_{\mathrm{L}}(\cos\theta_{3,i}\cos\theta_{4,i}\cos\theta_{\mathrm{H}}-\sin\theta_{3,i}\sin\theta_{\mathrm{H}})+\sin\theta_{\mathrm{L}}(\cos\theta_{4,i}\cos\theta_{\mathrm{H}}\sin\theta_{3,i} \\
\qquad +\cos\theta_{3,i}\sin\theta_{\mathrm{H}}) \\
\lambda x_{\mathrm{c},5,i} = -\sin\theta_{\mathrm{H}}(\cos\theta_{4,i}\cos\theta_{\mathrm{L}}\sin\theta_{2,i}+\sin\theta_{4,i}(\cos\theta_{2,i}\cos\theta_{\mathrm{L}}\sin\theta_{3,i}-\cos\theta_{3,i}\sin\theta_{\mathrm{L}})) \\
\lambda z_{\mathrm{c},5,i} = -\cos\theta_{\mathrm{H}}(\cos\theta_{4,i}\cos\theta_{\mathrm{L}}\sin\theta_{2,i}+\sin\theta_{4,i}(\cos\theta_{2,i}\cos\theta_{\mathrm{L}}\sin\theta_{3,i}-\cos\theta_{3,i}\sin\theta_{\mathrm{L}})) \\
\lambda \alpha_{\mathrm{c},5,i} = L\cos\theta_{\mathrm{H}}(\cos\theta_{\mathrm{L}}\sin\theta_{2,i}\sin\theta_{4,i}\sin\theta_{\mathrm{H}}+\cos\theta_{2,i}\cos\theta_{\mathrm{L}}(\cos\theta_{3,i}\cos\theta_{\mathrm{H}} \\
\qquad -\cos\theta_{4,i}\sin\theta_{3,i}\sin\theta_{\mathrm{H}})+\sin\theta_{\mathrm{L}}(\cos\theta_{\mathrm{H}}\sin\theta_{3,i}+\cos\theta_{3,i}\cos\theta_{4,i}\sin\theta_{\mathrm{H}})) \\
\lambda x_{\mathrm{c},6,i} = -\cos(\theta_{5,i}+\theta_{\mathrm{H}})(\cos\theta_{4,i}\cos\theta_{\mathrm{L}}\sin\theta_{2,i}+\sin\theta_{4,i}(\cos\theta_{2,i}\cos\theta_{\mathrm{L}}\sin\theta_{3,i}-\cos\theta_{3,i}\sin\theta_{\mathrm{L}})) \\
\lambda y_{\mathrm{c},6,i} = -\cos\theta_{\mathrm{L}}\sin\theta_{2,i}\sin\theta_{4,i}\sin\theta_{\mathrm{H}}+\cos\theta_{2,i}\cos\theta_{\mathrm{L}}(-\cos\theta_{3,i}\cos\theta_{\mathrm{H}}+\cos\theta_{4,i}\sin\theta_{3,i}\sin\theta_{\mathrm{H}}) \\
\qquad -\sin\theta_{\mathrm{L}}(\cos\theta_{\mathrm{H}}\sin\theta_{3,i}+\cos\theta_{3,i}\cos\theta_{4,i}\sin\theta_{\mathrm{H}}) \\
\lambda z_{\mathrm{c},6,i} = \sin(\theta_{5,i}+\theta_{\mathrm{H}})(\cos\theta_{4,i}\cos\theta_{\mathrm{L}}\sin\theta_{2,i}+\sin\theta_{4,i}(\cos\theta_{2,i}\cos\theta_{\mathrm{L}}\sin\theta_{3,i}-\cos\theta_{3,i}\sin\theta_{\mathrm{L}})) \\
\lambda \alpha_{\mathrm{c},6,i} = -L\sin(\theta_{5,i}+\theta_{\mathrm{H}})(\cos\theta_{\mathrm{L}}\sin\theta_{2,i}\sin\theta_{4,i}\sin\theta_{\mathrm{H}}+\cos\theta_{2,i}\cos\theta_{\mathrm{L}}(\cos\theta_{3,i}\cos\theta_{\mathrm{H}} \\
\qquad -\cos\theta_{4,i}\sin\theta_{3,i}\sin\theta_{\mathrm{H}})+\sin\theta_{\mathrm{L}}(\cos\theta_{\mathrm{H}}\sin\theta_{3,i}+\cos\theta_{3,i}\cos\theta_{4,i}\sin\theta_{\mathrm{H}})) \\
\lambda \gamma_{\mathrm{c},6,i} = -L\cos(\theta_{5,i}+\theta_{\mathrm{H}})(\cos\theta_{\mathrm{L}}\sin\theta_{2,i}\sin\theta_{4,i}\sin\theta_{\mathrm{H}}+\cos\theta_{2,i}\cos\theta_{\mathrm{L}}(\cos\theta_{3,i}\cos\theta_{\mathrm{H}} \\
\qquad -\cos\theta_{4,i}\sin\theta_{3,i}\sin\theta_{\mathrm{H}})+\sin\theta_{\mathrm{L}}(\cos\theta_{\mathrm{H}}\sin\theta_{3,i}+\cos\theta_{3,i}\cos\theta_{4,i}\sin\theta_{\mathrm{H}}))
\end{cases} \tag{A2}$$

References

1. Skormin VA, Nikulin V, Nicholson DJ. Omni-Wrist III-a new generation of pointing devices Part II gimbals systems-control. *IEEE T Aero Elec Sys* 2006;**42**(2):726–34.
2. Mauro S, Battezzato A, Biondi G. Design and test of a parallel kinematic solar tracker. *Mech Eng* 2015;**7**(12):1–16.
3. Li JJ, Jia YH. Configuration design of X-Y style antenna pedestal. *Elec Mech Eng* 2014;41–4.
4. Wu J, Chen XL, Wang LP. Design and dynamics of a novel solar tracker with parallel mechanism. *IEEE-ASME T Mech* 2016;**21**(1):88–97.
5. Ding HF, Huang P, Liu JF. Automatic structural synthesis of the whole family of planar 3-degrees of freedom closed loop mechanisms. *J Mech Robot* 2013;**5**(4), 0410061-10.
6. Yang SF, Sun T, Huang T. A finite screw approach to type synthesis of three-DOF translational parallel mechanisms. *Mech Mach Theory* 2016;**104**:405–19.
7. Wu C, Liu XJ, Wang LP. Optimal design of spherical 5R parallel manipulators considering the motion/force transmissibility. *J Mech Des* 2010;**132**, 0310021-10.
8. Dong X, Yu JJ, Chen B, Zong GH. Geometric approach for kinematic analysis of a class of 2-DOF rotational parallel manipulators. *Chin J Mech Eng* 2012;**25**(2):241–7.
9. Song YM, Yang Q, Dong G. Type synthesis of 2-DoF rotational parallel mechanism actuating the inter-satellite link antenna. *Chin J Aeronaut* 2016;**29**(6):1795–805.
10. Qi Y, Sun T, Song YM. Type synthesis of parallel tracking mechanism with varied axes by modeling its finite motions algebraically. *ASME Trans J Mech Robot* 2017;**9**(5), 0545041-6.
11. Zhong GY, Wang CQ, Yang SF. Position geometric error modeling, identification and compensation for large 5-axis machining center prototype. *Int J Mach Tools Manuf* 2015;**89**:142–50.
12. Wu JF, Zhang R, Wang RH. A systematic optimization approach for the calibration of parallel kinematics machine tools by a laser tracker. *Int J Mach Tools Manuf* 2014;**86**:1–11.

Please cite this article in press as: ZHANG J et al. Geometric error analysis of an over-constrained parallel tracking mechanism using the screw theory, *Chin J Aeronaut* (2018), https://doi.org/10.1016/j.cja.2018.08.021

13. Chen IM, Yang GL, Tan CT. Local POE model for robot kinematic calibration. *Mech Mach Theory* 2001;**36**:1215–39.
14. Whitney DE, Lozinski CA, Rourke JM. Industrial robot forward calibration method and results. *J Dyn Sys* 1986;**108**:1–8.
15. Xu QS, Li YM. Error analysis and optimal design of a class of translational parallel kinematic machine using particle swarm optimization. *Robotica* 2009;**27**:67–78.
16. Harb SM, Burdekin M. A systematic approach to identify the error motion of an N -degree of freedom manipulator. *Int J Adv Manuf Technol* 1994;**9**(2):126–33.
17. Wang J, Masory O. On the accuracy of a stewart platform-part I: the effect of manufacturing tolerances. *Proceedings of IEEE International Conference on Robotics and Automation*; 1993 Oct 14–17; Alanta, Georgia, USA; 1993. p. 114–20.
18. He B, Zhang PC, Hou SC. Accuracy analysis of a spherical 3-DOF parallel underactuated robot wrist. *Int Adv Manuf Technol* 2015;**79**:395–404.
19. Wang Y, Pessi P, Wu H. Accuracy analysis of hybrid parallel robot for the assembling of iter. *Fusion Eng Des* 2009;**84**(7–11):1964–8.
20. Chen GL, Wang H, Lin ZQ. Determination of the identifiable parameters in robot calibration based on the POE formula. *IEEE T Robot* 2014;**30**(5):1066–77.
21. Stone HW. *Kinematic modeling, identification, and control of robotic manipulators*. Dordrecht: Kluwer Academic Publishers; 1987. p. 293–306.
22. Zhuang H, Roth ZS, Hamano F. A complete and parametrically continuous kinematic model for robot manipulators. *IEEE Trans Rob Autom* 1992;**8**(4):451–63.
23. Fu GQ, Fu JZ, Xu YT. Product of exponential model for geometric error integration of multi-axis machine tools. *Int J Adv Manuf Technol* 2014;**l71**:1653–67.
24. Okamura K, Park FC. Kinematic calibration and product of exponential formula. *Robotica* 1996;**14**:415–21.
25. Park FC, Okamura K. *Kinematic calibration and product of exponential formula. Advances in robot kinematics and & computational geometry*. Cambridge: MIT Press; 1994. p. 119–28.
26. Frisoli A, Solazzi M, Pellegrinetti D. A screw theory method for the estimation of position accuracy in spatial parallel manipulators with revolute joint clearances. *Mech Mach Theory* 2011;**46**:1929–49.
27. Yang SF, Sun T, Huang T. Type synthesis of parallel mechanisms having 3T1R motion with variable rotational axis. *Mech Mach Theory* 2017;**109**:220–30.
28. Sun T, Yang SF, Huang T. A way of relating instantaneous and finite screws based on the screw triangle product. *Mech Mach Theory* 2017;**108**:75–82.
29. Charker A, Mlika A, Laribi MA. Accuracy analysis of non-overconstrianed spherical parallel manipulators. *Eur J Mech A-Solid* 2014;**47**:362–72.
30. Kumaraswamy U, Shunmugam MS, Sujatha S. A unified framework for tolerance analysis of planar and spatial mechanisms using screw theory. *Mech Mach Theory* 2013;**69**:168–84.
31. Liu HT, Huang T, Derek GC. A general approach for geometric error modeling of lower mobility parallel manipulators. *J Mech Robot* 2011;**3**:021013–21034.
32. Sun T, Zhai YP, Song YM. Kinematic calibration of a 3-DoF rotational parallel manipulator using laser tracker. *Robot Com-Int Manuf* 2016;**41**:78–91.
33. Sun T, Song YM, Li YG. Dimensional synthesis of a 3-DOF parallel manipulator based on dimensionally homogeneous Jacobian matrix. *Sci China-Technol Sci* 2010;**53**(1):168–74.
34. Jiang Y, Li T, Wang L. Kinematic error modeling and identification of the over-constrained parallel kinematic machine. *Robot Comput-Integrated Manuf* 2018;**49**:105–19.
35. Dai JS, Huang Z, Lipkin H. Mobility of overconstrained parallel mechanisms. *Trans ASME J Mech Des* 2004;**128**(1):220–9.
36. Xu YD, Liu WN, Yao JT, Zhao YS. A method for force analysis of overconstrained lower mobility parallel mechanism. *Mech Mach Theory* 2015;**88**:31–48.
37. Liu WL, Xu YD, Yao JT, Zhao YS. The weighted Moore-Penrose generalized inverse and the force analysis of overconstrained parallel mechanisms. *Multibody Syst Dyn* 2017;**39**(4):363–83.
38. Li J, Xie F, Liu XJ. Geometric error modeling and sensitivity analysis of a five-axis machine tool. *Int J Adv Manuf Technol* 2016;**82**(9):1–15.
39. Caro S, Wenger P, Bennis F. Sensitivity analysis of the Orthoglide: a three-DOF translational parallel kinematic machine. *J Mech Des* 2006;**128**:392–402.
40. Wu WD, Rao SS. Interval approach for the modeling of tolerances and clearances in mechanism analysis. *J Mech Des* 2004;**126**:581–92.
41. Zhang D, Gao Z. Optimal kinematic calibration of parallel manipulators with pseudoerror theory and cooperative coevolutionary network. *IEEE Trans Ind Electron* 2012;**59**(8):3221–31.
42. Chen YZ, Xie FG, Liu XJ. Error modeling and sensitivity analysis of a parallel robot with SCARA (Selective Compliance Assembly Robot Arm) motions. *Chin J Mech Eng* 2014;**27**(4):693–702.
43. Qi Y, Sun T, Song Y. Multi-objective optimization of parallel tracking mechanism considering parameter uncertainty. *J Mech Robot* 2018;**10**(4), 0410061-11.

Please cite this article in press as: ZHANG J et al. Geometric error analysis of an over-constrained parallel tracking mechanism using the screw theory, *Chin J Aeronaut* (2018), https://doi.org/10.1016/j.cja.2018.08.021